eprints@whiterose.ac.uk
https://eprints.whiterose.ac.uk/

Combined influence of carbonation and leaching on freeze-thaw resistance of limestone ternary cement concrete

Samuel Adu-Amankwah[1], Maciej Zajac[2], Jan Skoček[2], Jiří Němeček[3], Mohsen Ben Haha[2], Leon Black[1]

[1]School of Civil Engineering, University of Leeds, Woodhouse Lane, LS29JT

[2]HeidelbergCement Technology Center GmbH, Oberklamweg 2-4, 69181 Leimen, Germany

[3]Czech Technical University in Prague, Faculty of Civil Engineering, Thakurova 7, 16629 Prague 6, Czech Republic

Abstract

Performance of OPC and composite cements including limestone ternary blended concretes and pastes exposed to natural carbonation, leaching, and freeze-thaw (FT) cycles and their coupling were investigated. The combined regime is analogous to the Capillary suction, internal damage and Freeze-thaw (CIF) test. The freeze-thaw results showed that composite cement concretes are more susceptible to surface scaling and internal damage. Microanalysis of complementary cement pastes revealed partial carbonation after equilibration at 65% RH. Decalcification due to leaching accompanied capillary suction, profound in the partially carbonated ternary cement pastes such that portlandite was depleted from the surface before the FT cycles commenced. Successive cycles increased porosity; heterogeneity and coarsening of the pore structures were drastic when carbonation and leaching preceded FT, modifying the C-S-H morphology and composition. Curtailing carbonation and leaching reduced surface scaling and internal damage to comparable levels as OPC of the same strength class. These findings imply that changes in porosity and phase assemblage in composite cements caused by carbonation and leaching contributed to their FT susceptibility.

Keywords: *Limestone ternary cement; carbonation; leaching; freeze-thaw resistance; durability; microstructure*

1 Introduction

Freeze-thaw damage is a major durability concern for concrete structures in cold climates. Typical defects manifest in the form of surface scaling, internal damage, or their combination. De-icing salts and critical saturation are pre-requisites for the surface scaling form of freeze-thaw damage [1, 2]. This form of deterioration may not initially impair structural integrity, being just unsightly, but successive losses of material can eventually be detrimental, reducing the cover around reinforcing bars and accelerating other forms of deterioration. Internal structural damage meanwhile culminates in micro-cracks and, as a result, reduces durability and engineering performance. Whether the same mechanisms control these indicators of freeze-thaw damage remains contentious [3-7].

Freeze-thaw resistance of composite cement concretes has been the subject of several investigations [1, 8-13]. Laboratory data show that concretes with high slag [14-16] or limestone [17, 18] loading without adequate air entrainment are more susceptible to freeze-thaw damage, but the extent of damage is less drastic in complementary field exposed concrete [8, 14, 19]. This brings into question aspects of laboratory testing of FT that interfere with outcomes. For example, the capillary suction, internal damage and freeze-thaw (CIF) test

42   method stipulates 21-day equilibration at 65% RH and re-saturation of 7-day specimens before
43   exposing to FT cycles while ASTM C666 and C672 recommend 28-day drying in air at 50%
44   RH. Previous studies have demonstrated microstructural alterations caused by some of these
45   treatments [20-33], but the extent to which these influence freeze-thaw performance has not
46   been clarified. Such understanding is critical especially for composite cement concrete with
47   high clinker substitution since the above conditioning may significantly alter the
48   microstructures.

49   Microstructural aspects other than pore structures e.g. phase assemblages and their volume
50   and their implications on FT have received limited consideration. Some studies have
51   speculated the role of ionic migration during freeze-thaw [11, 13] while in-situ reactions
52   involving hydrated assemblages and other ions, e.g. carbonation and chlorides are also
53   reported [9, 12, 13, 19, 34]. Postulated FT mechanisms such as the hydraulic pressure, closed
54   container, microscopic ice-lens and the glue-spall hypotheses [2, 35-38] do not explain such
55   ionic interactions. The osmotic and crystallization pressure theories consider ionic interaction
56   in the degradation process but these assume migration of substances e.g. CO_2 and Cl- into
57   concrete [6, 7, 10, 11, 19]. Loss of species through leaching alters the microstructure and have
58   been reported to accelerate freeze-thaw damage [10, 13]. In examining the stability of air-
59   voids in concrete, Detwiler *et al.* [39] observed deposits of portlandite around air-void
60   perimeters, whilst increasing calcium concentration in the pores during freezing was reported
61   elsewhere [40, 41]. Given that composite cements are prone to carbonate due to low Ca
62   concentration with attendant coarsening of pore structures in addition to ionic transport during
63   FT cycles, the combined action of carbonation and leaching deserve thorough examination.
64   The objective of this contribution is to systematically investigate phase assemblages and pore
65   structural changes during equilibration and conditioning regimes of the FT test. The
66   experimental design allowed isolation of allied degradation mechanisms, and microstructural
67   findings were validated on concrete specimens.

2 Materials & Methods

Materials

70   Four concrete mixes were investigated; Portland cement, a binary slag blend, and two
71   limestone ternary composite cements, designated as C, CS, CSL and CS2L (where L and 2L
72   respectively indicate the presence of 10 and 20% limestone in the cement). The pure Portland
73   cement samples were prepared from CEM I 42.5 R according to BS EN 196-1, while CEM I
74   52.5 R cement was used in the composite cements. The clinker to SCM ratio was maintained
75   at 50:50, with limestone and slag considered as SCMs. The total sulfate content was
76   maintained at 3% by considering the sulphate content of the CEM I 52.5R with addition of
77   natural anhydrite to balance. The formulated cements were homogenized in a laboratory ball
78   mill, using polymer balls. Table 1 shows the chemical composition and specific surface area
79   of the materials, determined by XRF and Blaine measurements respectively.

80   Concrete mix design was by the yield method, taking into account the specific gravities of all
81   constituent materials. The w/c ratio for concrete was maintained at 0.5 with water absorption
82   by the aggregates accounted for in the mix design. The following predefined values were kept
83   constant in the mix designs: 320.3kg/m^3 cement, 2.5% total entrapped air and 0.54 fine to
84   coarse aggregate ratio. The coarse aggregates were quartzite, 20% of which was 10mm with

85 the remainder being 20mm. Air entrainment admixtures were not used in any of the mixes.
86 Table 2 shows the mix proportions per cubic metre.

87

88 **Table 1 Chemical composition (% weight) and Blaine fineness of the investigated materials**

Material	CEM I 42.5 R	CEM I 52.5 R	Slag	Limestone	Anhydrite
SiO_2	20	20.4	34.9	2	2
Al_2O_3	5.4	5.6	11.6	0.8	0.6
TiO_2	0.3	0.3	1.1		
MnO	0.1		0.3		
Fe_2O_3	2.6	2.5	0.5	0.3	0.2
CaO	62.5	62.1	41.8	53.1	38.3
MgO	1.4	1.7	5.8	0.6	1.5
K_2O	0.8	0.7	0.5	0.1	0.2
Na_2O	0.1				
SO_3	3.2	3.5	3.1		52.2
P_2O_5	0.2	0.1			
LOI (Others)	3.4	3.1	+1.5(0.4)	42.3 (0.8)	3.7 (1.3)
Blaine, m^2/kg	383	593	454	328	472

89

90 **Table 2 Concrete mix design (kg/m^3)**

Mix ID	CEMI	Slag	Limestone	Anhydrite	Effective water	Aggregates		
						Fine	10mm	20mm
C1	320.3	-	-	-	160.2	651.8	237.7	950.8
CS	162.3	150.8	-	7.2	160.2	648.8	236.6	946.4
CSL	163.9	121.8	27.4	7.2	160.2	648.1	236.4	945.5
CS2L	163.9	91.4	57.8	7.2	160.2	647.4	236.1	944.5

91 NOTE: The composite cements contained 3% sulfate content.

92 **Methods**

93 ***Freeze-thaw test on concrete***

94 The FT test was performed according to a modified PD CEN/TR 15177:2006 [42] in deionized
95 water using the CIF method. The concrete specimens were made according to BS EN 12390-
96 2. The 150mm cubes were split into two using PTFE sheets. After demoulding, the specimens
97 were cured for 6 days and conditioned at 65% RH, 20ºC for 21-days. The lateral sides of the
98 specimens were thereafter sealed using a 2-part epoxy resin before commencing the 7-day
99 capillary suction in deionized water. The specimens were then subjected to 56 FT cycles in
100 deionized water according to the profile shown in Figure 1. In our setup, one FT cycle lasted
101 24-hours instead of 12-hours in the CIF test method [42]. The cycle is consistent with that

102 used in the slab test and reflects the typical day and night winter cycles. However, duration at
103 the minimum temperature was kept consistent at 3-4 hours. Freeze-thaw damage was
104 assessed in terms of the water uptake by the specimens, scaled matter and internal structural
105 damage. The scaled mass was collected at regular intervals during the test. The test
106 containers and specimens were subjected to 3 minutes cleaning in a sonic bath and the scaled
107 matter washed on a filter paper. These were dried to constant mass in a glovebox on a hot
108 plate at 40°C. Internal structural damage was assessed in terms of the relative dynamic
109 modulus (RDME) based on the mean transit time of wave pulses through the specimens.
110 Additionally, the water uptake was evaluated from the mass change in the specimens during
111 the test, measured on a weighing balance with 0.1g accuracy. The water suction time was
112 taken as the sum of the re-saturation and the cumulative thawing time of 7-hours per cycle
113 [43].
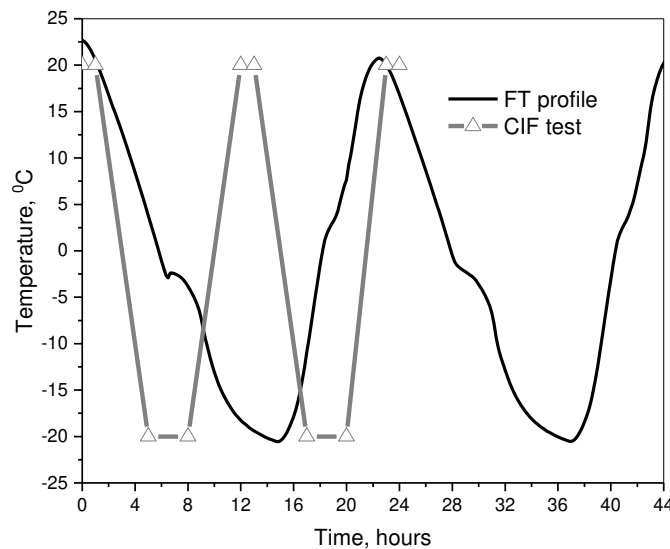
Figure 1 Temperature profile for the FT test as measured in the test solution

Freeze-thaw test on cement pastes

117 Initial studies with the cement pastes revealed sequential removal of surface matter, as
118 illustrated in Figure 2. Significant cracks formed initially in the outer 2 – 4mm layers with
119 successive FT cycles. The material contained within the cracks spalled eventually, exposing
120 the layers underneath for a repetition of the cycle. Subsequently, full-scale experiments were
121 designed to study the microstructures of the outer surfaces and cores of the cement pastes
122 as a function of the specimen conditioning and FT environment, as shown schematically in
123 Figure 3. Complementary cement paste samples were prepared using a vortex mixer from the
124 mix design shown in Table 2but without aggregates. The cement pastes were cast into 25mm
125 diameter plastic vials. These were stored on a lab rotator for 24 hours to minimize bleeding
126 before being transferred to a water-bath maintained at 20°C for 6-days. To simulate the
127 surface and core of the samples in line with observations from Figure 2, two sets of 7-day old
128 paste samples were crushed into 1 – 2mm thick particles. The sets mirroring the outer layers
129 were conditioned and exposed as per the CIF method (i.e. equilibrated at 65% RH and 20°C
130 under atmospheric CO_2, designated as CIF. Meanwhile, those corresponding to the core were
131 kept sealed until 28-days. Both sets were saturated and subsequently exposed to cyclic FT
132 conditions in:

133   (i)   Deionized water (designated as CIF-DI) to clarify the impact of carbonation during
134   equilibration on FT, and
135   (ii)   Saturated lime solution (designated as series CIF-L) to differentiate the effect of
136   leaching. The comparison between series CIF-L and series CIF gave a basis to
137   assess the coupled effect of carbonation and leaching.

0 FT   11FT   25 FT
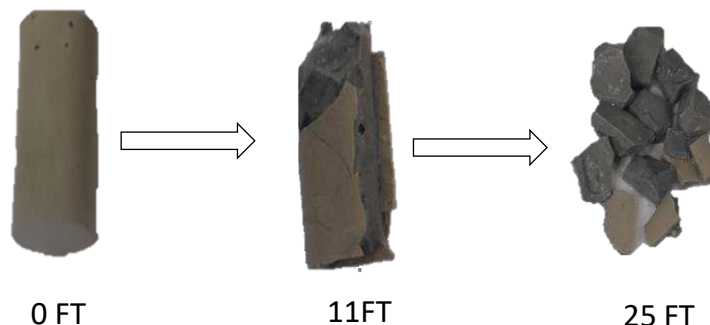
138

139   **Figure 2 Sequence of FT on cement pastes**

140

Series	Conditioning	Capillary suction and FT testing
CIF	65% RH, 20°C in ambient air	Deionised water
CIF-DI	sealed	Deionised water
CIF-L		Saturated lime solution

7d	7d-21d exp	7d sat-0 FT	7d sat-25 FT
	28d sealed		

141   **Figure 3 Schematic of the equilibration and FT testing regimes of the cement pastes**

142   Note: Key stages of characterization are marked with the boxes

143

144   In all cases, the re-saturation and FT tests were performed at a solid/liquid ratio of 1:500 and
145   the test solutions were renewed weekly. The solids comprised the crushed paste samples and
146   5mm thick slices for subsequent indentation measurements and scanning electron
147   microscopy. At the required stage, about 10g of the crushed paste samples for TGA, XRD and
148   MIP and slices for SEM were hydration stopped by double solvent exchange. For TGA and
149   XRD, the crushed pastes samples were ground in iso-propanol (IPA) for 20 minutes, but for
150   24 hours for the MIP and SEM specimens. The IPA was filtered under gravity followed by
151   flushing with diethyl-ether. The residue was subsequently dried on a hot plate heated at 40°C
152   for 10 minutes. The specimens were subsequently stored in mini-grip bags until testing. The
153   procedure was carried out inside a glove-box which was kept free of CO_2 by purging with
154   nitrogen gas.

155   TGA was performed on a Stanton Redcroft 780 Series Analyser under nitrogen. About 16-18
156   mg of additionally ground powder sample was heated in a platinum crucible at a rate of 20
157   °C/minute up to 1000°C. The portlandite and calcium carbonate contents were computed
158   between ~400-500°C and ~650–800°C from the TGA trace using equations (1-2) respectively.

159 The contents were normalized to the ignited weight at 550°C for portlandite and 1000ºC for
160 calcium carbonate.

$$CH = \frac{CH_{TG}\,{}^{74}/_{18}}{M_{550^0C}} * 100\% - - - - - - - (1)$$

$$Cc = \frac{Cc_{TG}\,{}^{100}/_{44}}{M_{1000^0C}} * 100\% - - - - - - - (2)$$

163 Note, CH is portlandite content, CH_{TG} is % weight loss due to water in calcium hydroxide, Cc
164 is calcium carbonate content and Cc_{TG} is the % weight loss due to CO_2 in calcium carbonate,
165 $M_{550°C}$ is the ignited weight at 550°C and $M_{1000°C}$, the ignited weight at 1000°C. Note that the
166 tangent method was used to calculate the mass losses CH_{TG} and Cc_{TG} from the TG curves.

167 XRD scans were acquired on a Bruker D2 Phaser benchtop diffractometer equipped with a
168 Lynxeye detector using a CuKα anode operating at 30 kV and 10 mA. The scans were
169 performed with a step size of 0.0334° over a range of 5-70 °2θ. TOPAS Academic software
170 v4.2 was used to quantify the phase contents at the key stages in Figure 2 including the
171 residual slag content. The refinement procedure, based on the external standard method is
172 detailed elsewhere [44]. The bound water content was used to correct x-ray absorption in the
173 attenuation co-efficient calculations. Subsequently, the refinement results after each stage of
174 the test was rescaled to 100g of the paste. Accuracy of the QXRD calculations for the
175 crystalline phases is ± 1% and that of the GGBS is ± 2%.

176 MIP measurements were performed on 1 – 2mm thick crushed samples using a
177 Quantachrome Instruments' PoreMaster-60. Approximately 1 g of sample was intruded with
178 mercury at the rate of 6-19 MPa/min up to 400 MPa at 22°C. The intrusion data was converted
179 to cumulative pore volume using the cylindrical and plate model together with the Washburn
180 equation, taking the contact angle and the surface tension of mercury as 140° and 0.48 N/m
181 respectively. The data is presented in terms of the cumulative intruded volume and derivative
182 after smoothening by the adjacent averaging method. The pores were subsequently classified
183 according to [45].

184 ***Micro-indentation***

185 Micro-indentation measurements were performed on the series CIF paste samples after
186 equilibration and before capillary suction (i.e. 7d-21d exp) and then after 25 FT cycles (i.e. 7d-
187 21d exp-7d sat-25FT). The 5mm thick slices were hydration-stopped by freeze-drying to
188 constant mass, then impregnated in resin. After setting, the samples were ground on silicon-
189 carbide abrasive paper and an intermediate non-woven pressed cloth but without scratch
190 remover to minimize artefacts on the surface. The indents were prescribed in a rectangular
191 grid of 10 x 10-indents with 75-100 micrometer spacing, i.e. covering a large portion of surface
192 including variety of microstructural phases. CSM nano-hardness tester with a corner cube
193 indenter was used. The surface roughness was estimated (based on optical imaging) to be in
194 the range of tens to hundreds of nanometres over a 50x50 micrometer area. Consequently, a
195 relatively large indentation depth (in the scale of 10 micrometers) was implemented to
196 minimize the influence of uneven surfaces and obtain effective properties from a larger volume
197 ($\sim$50x50x50 μm^3). As a result, the majority of indents were produced within the matrix and the
198 results characterize the matrix properties. A typical grid and a single point indent at a higher
199 magnification are shown in Figure 4.

The high magnification image in Figure 4 indicates a regular indent shape, meaning the local roughness was acceptable in the scale [46]. However, heterogeneity due to intermixing of hydrates and unreacted grains was noticed. Consequently, some fluctuations in the results were anticipated. The indentation data are presented in terms of the Young's modulus (E_{it}) derived from the reduced modulus (E_r) according to [47].
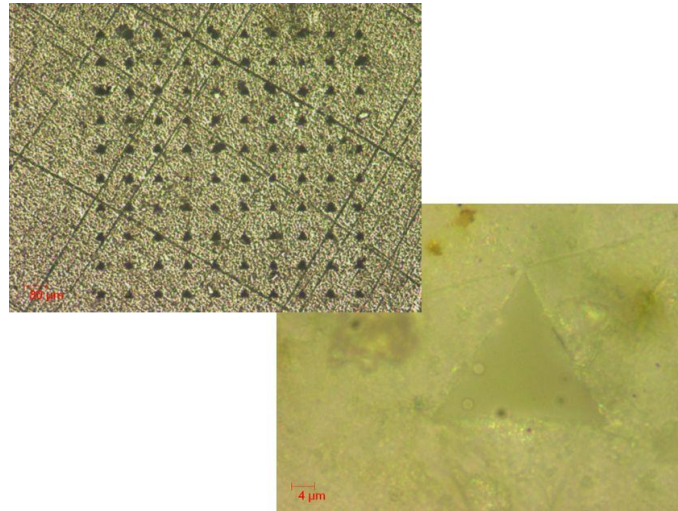
Figure 4 Micro-indentation grid and magnified image of the indent

3 Results and discussion

3.1 Freeze-thaw performance of concrete in deionized water

Figure 5 (a – d) shows representative photographs of concrete samples taken after 56 FT cycles. Meanwhile, the extent of surface scaling is shown in Figure 6. These reveal surface scaling in all concretes, irrespective of the cement type. The damage was more pronounced in the composite cement concretes, more so in the limestone containing mixes. Increasing the limestone content from 10 to 20% further increased scaling. A lower resistance to scaling in concrete containing more than 45% GGBS or 10% limestone contents were reported elsewhere [3, 16, 18]. However, the observation of surface scaling among concrete samples subjected to FT in deionized water is in contrast with suggestions that the presence of de-icing salts is a pre-requisite for surface scaling [1, 2, 5, 7]

Internal damage and water uptake during the FT exposures are also shown in Figures 6 and 7. In all mixes, significant internal damage preceded surface scaling. The onset of internal damage, as revealed by the reducing RDME, commenced sooner in the composite cement concrete, while the neat cement mix did not experience any measurable damage until after 28 FT cycles. Not only were the composite cement mixes more susceptible, but the presence of limestone further accelerated internal damage such that, these were already below the 80% failure criterion [48] by the 28th FT cycle.
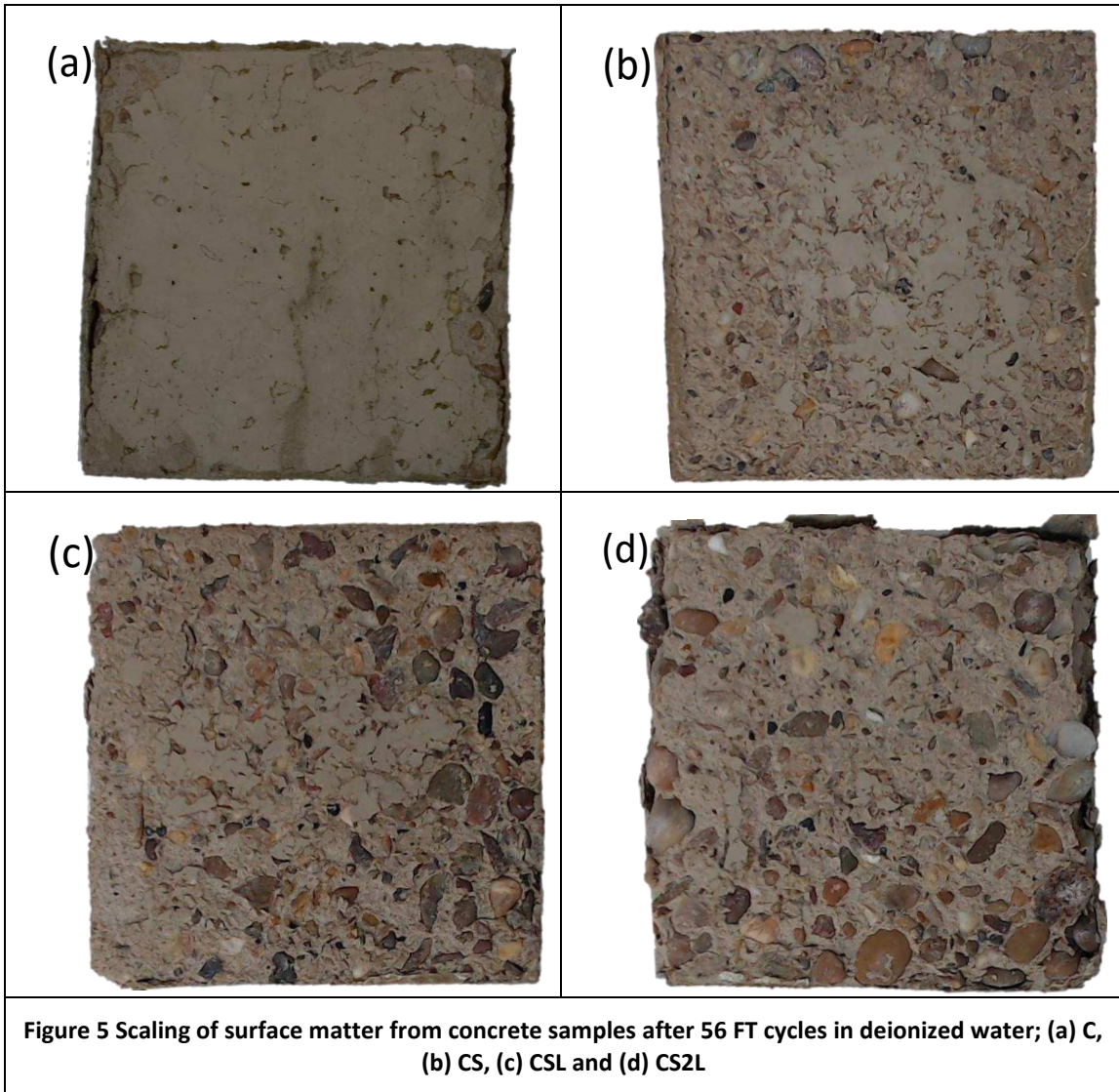
Figure 5 Scaling of surface matter from concrete samples after 56 FT cycles in deionized water; (a) C, (b) CS, (c) CSL and (d) CS2L

226
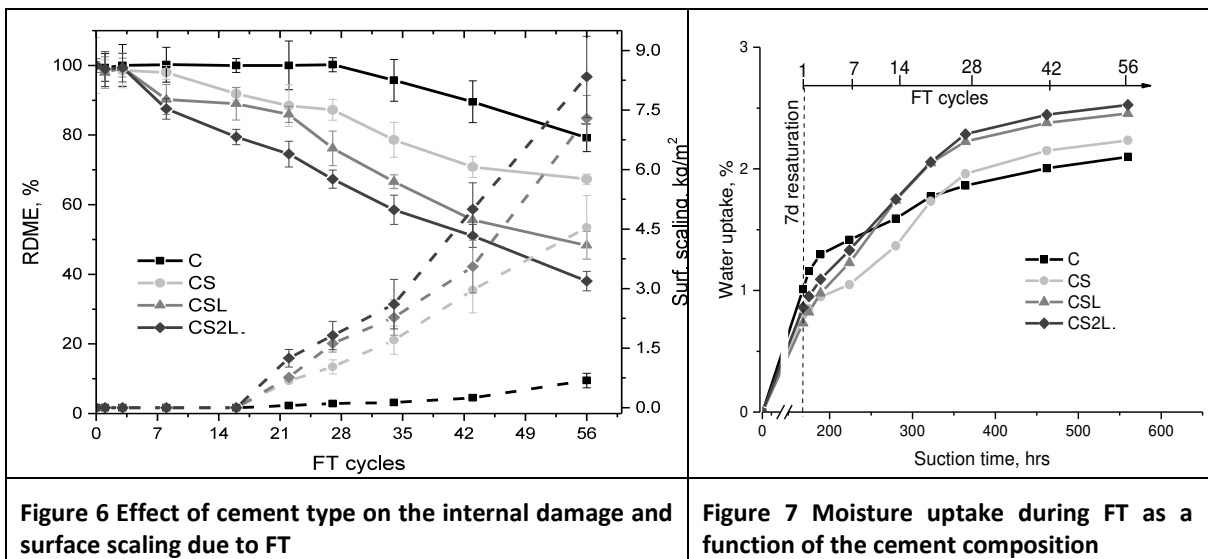
Figure 6 Effect of cement type on the internal damage and surface scaling due to FT

Figure 7 Moisture uptake during FT as a function of the cement composition

227

228 Figure 7 shows significant moisture uptake occurred in all concrete during the initial 7-day
229 capillary suction, though at different rates. The trends continued during FT, with the so called
230 pumping effect caused by contraction of the matrix during thawing , as well as micro-cracks
231 arising from internal damage, contributing to an increased suction of the test solution into the
232 concrete. These observations reflect the extent of internal damage among the samples, being
233 greatest in the limestone ternary cements. Weight gain due to capillary suction was highest in
234 the composite cement mixes compared to the neat cement mix. It is noteworthy that a higher
235 apparent sorptivity was measured in the latter mixes [49]. Consequently, damage induced by
236 FT seems to account for the higher moisture uptake in the composite cement concrete.

237 A point of interest in the water-uptake profiles is the time to reach the 'nick point' on the water-
238 uptake vs. time curve. This point is indicative of critical saturation of the matrix ; after which
239 further moisture uptake should slow down considerably, unless exacerbated by pressure and
240 associated micro-cracks. From Figure 7, the time to reach the nick-point coincided with the
241 onset of internal damage in mix C. However, in the composite cement concrete, significant
242 internal damage had already occurred before the 'nick-point'. This suggests that the water
243 uptake-internal damage correlation during FT, as reported elsewhere [43], is less relevant in
244 these mixes. Evidence of internal damage after a couple of FT cycles in the composite cement
245 mixes suggests the matrix was perhaps critically saturated after the initial 7-day re-saturation.
246 Further evaluation of the phase assemblages and pore structure is needed to clarify the
247 underlying factors for these observations.

248 3.2 Microstructural changes at the paste level

249 The above observations warrant a critical evaluation of the interplay between cement
250 composition and FT resistance of concrete. The cements investigated here differed with
251 respect to the contents of hydrated phase assemblages and pore structures [44, 50].To
252 elucidate the extent and mechanism of interaction between these, FT tests were designed to
253 separate the inherent microstructural effects from those changes induced by the test regime
254 including potential carbonation and leaching as illustrated in Figure 3. The results are
255 presented in terms of the changes in the phase assemblages and pore structures focusing on
256 mixes C and CSL at stages of the test illustrated in Figure 3 and without carbonation and or
257 leaching.

258 3.2.1 Microstructure of partially carbonated cement pastes subjected to FT in deionized
259 water (CIF method): Series CIF

260 Phase assemblages

261 The capillary suction, internal damage and freeze-thaw (CIF) test method used to investigate
262 the concrete specimens required 7-day moist curing followed by equilibration for 21 days at
263 65% RH and 20°C before exposure to the FT cycles. The protocol mimics natural exposure
264 and hence does not take into account carbonation of the specimens. Important questions
265 therefore arise concerning the extent of carbonation during equilibration and its impact on
266 resistance to subsequent FT cycling.

267 DTG plots in Figure 8 (a and b) reveal systematic differences in the hydrate contents (i.e. C-
268 S-H, ettringite, Hc/Mc and CH) as well as the calcium carbonate signatures. There was a
269 significant reduction in the signals due to C-S-H and ettringite after equilibration, irrespective
270 of the type of cement. Meanwhile, more calcium carbonate formed while portlandite

diminished. The former decomposed at lower temperatures, suggestive of metastable calcium carbonate, consistent with [51]. However, carbonation alone does not explain the significant changes in the C-S-H signals. Portlandite in both mixes after equilibration implies buffering against carbonation of the C-S-H and ettringite. However, simultaneous carbonation of portlandite and other calcium bearing assemblages e.g. C-S-H, ettringite have been noted elsewhere [52]. The x-ray diffraction patterns (Figure 9 a and b) corroborate reduced ettringite contents, and calcite formation from portlandite. However, changes in the AFm phases were slight, from both DTG and XRD data.

Besides equilibration, Figure 8 further reveals modifications in the hydrated assemblages upon saturation in deionized water. DTG and XRD both showed more C-S-H, ettringite and AFm (particularly Mc) in both cements. Unlike CSL, over 50% of the pre-equilibration portlandite content was still present in mix C after the initial capillary suction. The calcite content however increased upon saturation due to crystallization of the carbonate polymorphs formed from equilibrating the samples at 65% RH. This is consistent with the DTG in Figure 8 and the findings of Dubina *et al.* [53] who observed a shift towards crystalline carbonates with increasing relative humidity.
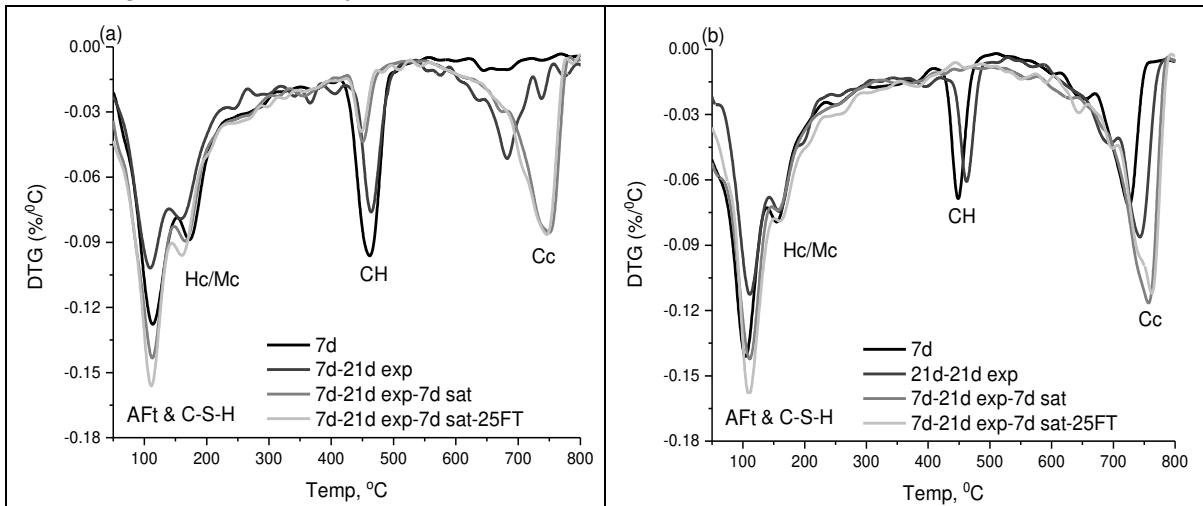
Figure 8 DTG trace of samples tested according to series CIF (a) mix C, (b) mix CSL
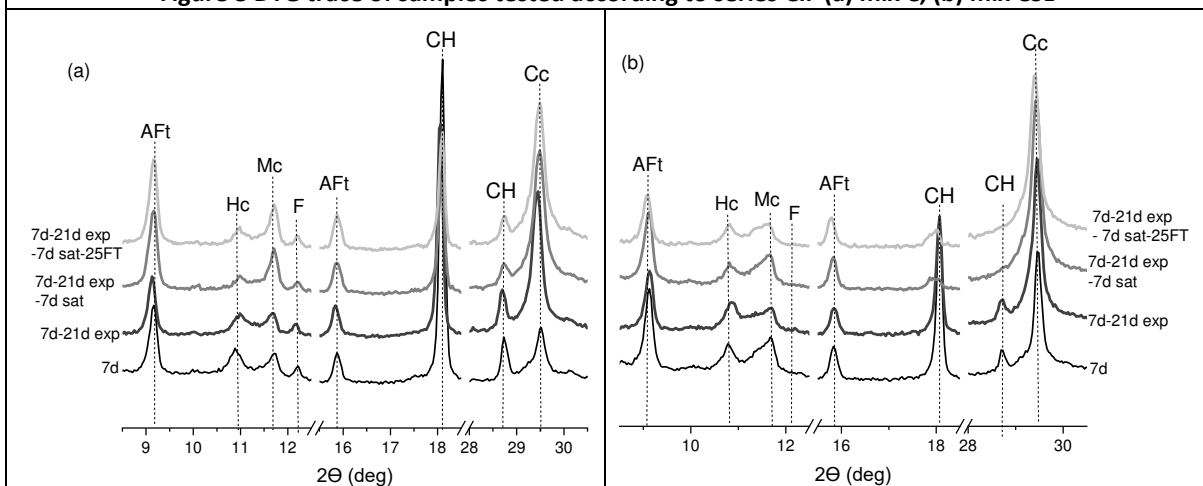
Figure 9 XRD plots of samples tested according to series CIF (a) mix C, (b) mix CSL

288　QXRD (Figure 10) facilitates examination of the changes in the residual phase assemblages.
289　In interpreting the results, one must however recognize that these specimens constituted an
290　open system, in that, hydration, carbonation, and leaching occurred simultaneously, as
291　noticed in Figure 8 and 9.

292　Figure 10 (a and b) confirm lower ettringite contents in both cements after equilibration.
293　Meanwhile, portlandite was lost from both systems upon exposure to deionised water, with
294　the formation of calcite, but the loss was complete in the ternary blend. In mix C,
295　monocarboaluminate (Mc) formed at the expense of hemicarboaluminate (Hc) but these
296　phases co-existed in mix CSL. The increased calcite and x-ray amorphous phase contents
297　over this period indicate a combination of carbonation and potential alterations in crystallinity
298　of some assemblages due to drying and/or carbonation.
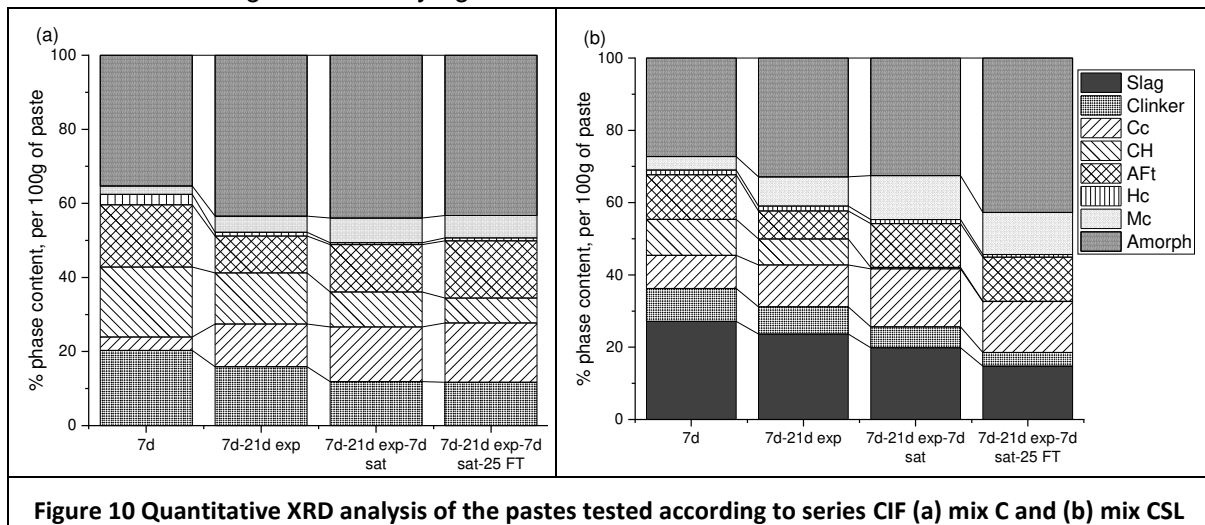
Figure 10 Quantitative XRD analysis of the pastes tested according to series CIF (a) mix C and (b) mix CSL

299

300　The extent of clinker and slag hydration during the 7-day capillary suction were within the
301　accuracy of the QXRD technique. However, continued hydration during FT is evident from the
302　residual clinker and slag contents at the end of the test. Additional ettringite precipitated after
303　saturation and stabilized during FT such that the contents were comparable or greater than
304　the levels prior to equilibration, as reflected in Figure 8. Partial decomposition and
305　reprecipitation of ettringite as a function of RH was noticed elsewhere [24, 25]. Meanwhile, the
306　monocarboaluminates contents became more prevalent but the calcium carbonate content
307　increased concurrently (Figure 8). A significant increase in the XRD amorphous phase content
308　at the end of the test, prominently in mix CSL is noteworthy.

309　***Pore structure***

310　Modifications in the phase assemblages due to partial carbonation during equilibration,
311　saturation, and FT was reflected in the pore structures. The cement paste samples were
312　analysed after the stages in Figure 3 using mercury intrusion porosimetry. Figure 11 (a – d)
313　shows the cumulative intruded volumes and their derivatives.

314　Four main clusters of accessible pore sizes are noticed in the derivative plots, viz. pores < 10
315　nm, 10nm – 100nm, 100 nm – 1000 nm and > 1000 nm. Pores ranging between 10 -100 nm
316　dominated both cements. The prevalence of pores finer than 10 nm that characterized mix
317　CSL after 7-day moist curing is typical of slag containing cements [30, 31, 50, 54], attributable
318　to the intrinsic gel porosity of the additionally formed C-S-H.

319

Figure 11 MIP measurement of cement paste samples tested according to series CIF

Note: (a) Pore distribution of Mix C, (b) pore distribution of mix CSL, (c) cumulative intruded volume in mix C and (d) cumulative intruded volume in mix CSL
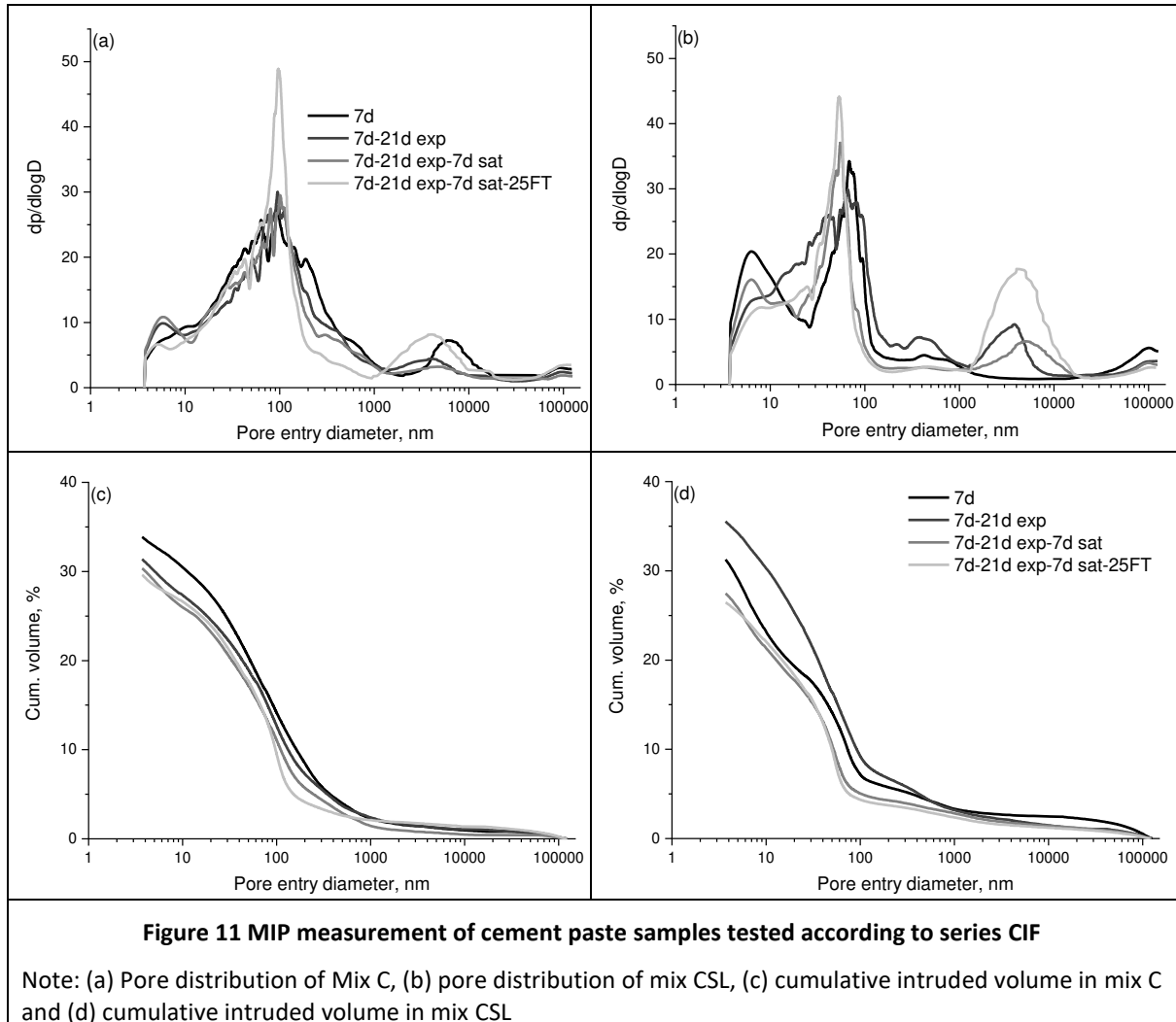
320

321 Equilibration in atmospheric CO_2 clogged the gel pores in mix CSL but the capillary pores
322 coarsened, leading to a significant increase in the total porosity. Conversely, the meso-
323 capillary pores (i.e. 10 – 30nm) were clogged in mix C after partial carbonation, but less than
324 reported elsewhere for mortar samples [30, 51]. Minimal changes in the gel porosity of mix C
325 indicates minimal carbonation of the C-S-H, potentially due to buffering by portlandite. A
326 corresponding reduction in the total porosity was noticed consequently. Distinctive to mix CSL
327 is the dominant cluster of micro capillary pores after equilibration. Such alterations in the pore
328 distributions have not been reported in previous carbonation studies on composite cements,
329 but the overall increase in porosity is consistent with the literature [30, 51, 52].

330 Figure 11 shows that the 7d capillary suction preceding the FT cycles caused moderate
331 refinement in the pore distribution in mix C but more significantly in mix CSL. In both cements
332 however, the volume of pores finer than 10nm increased after capillary suction, and the
333 subsequent FT cycles refined all pore ranges without a notable change in total porosity. The
334 micro-capillary pores were the only exception after FT, becoming dominant with increasing
335 cycles, more so in the limestone ternary cement.

3.2.2 Microstructure of non-carbonated cement paste samples subjected to FT in deionized water: Series CIF-DI

The preceding section highlighted modifications in the phase assemblages and pore structures induced by equilibration in atmospheric CO_2 and saturating the cements in deionized water as part of the FT test. The changes in microstructure and phase assemblage were significant, such that determining the reasons for resistance to FT could not be deciphered. In an attempt to separate the influence of carbonation from FT, paste samples, cured for 28-days in a non-carbonating atmosphere were saturated and subjected to FT cycles in de-ionized water. Subsequently, these were characterized using thermal analysis and XRD.

Figure 12 (a and b) reveals moderate increase in the C-S-H and ettringite signals in both cements. Figure 13 (a and b) meanwhile shows insignificant changes in the ettringite content while the XRD amorphous content increased. Consequently, the increased DTG signal indicate ongoing hydration and hence additional C-S-H and other assemblages. This is consistent with the increased portlandite content also.
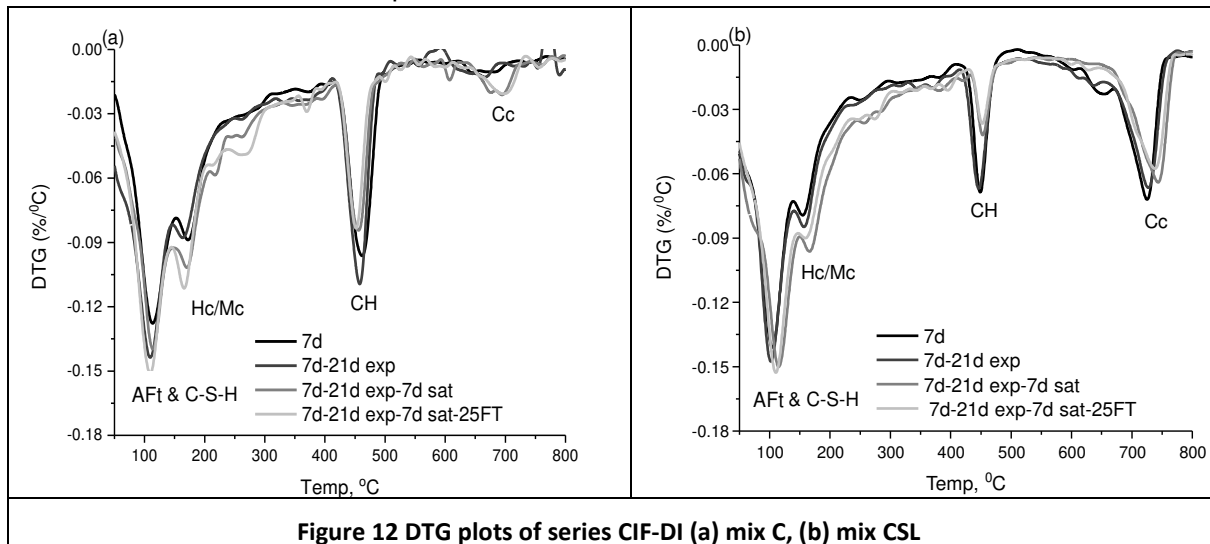
Figure 12 DTG plots of series CIF-DI (a) mix C, (b) mix CSL

Capillary suction before and during the FT cycles was accompanied by less drastic increase in the C-S-H and ettringite signals compared to series CIF. Figure 13 does not reveal additional ettringite upon saturation, instead an increase in the XRD amorphous content. Meanwhile, increasing AFm signatures continued through to saturation, but stabilized afterwards.

Portlandite loss due to saturation in deionized water occurred even before exposure to the FT cycles, but to a lesser extent compared to series CIF. About 50% of the portlandite in mix CSL was lost after the 7-day saturation but considerably more portlandite was still present in mix C. This implies that the severity of portlandite loss depended on the cement type and pre-exposure microstructures. Besides, additional monocarboaluminates formed while the x-ray amorphous content increased. Similar trends were observed after 25 FT cycles with appreciable increase in the x-ray amorphous content in both cements.
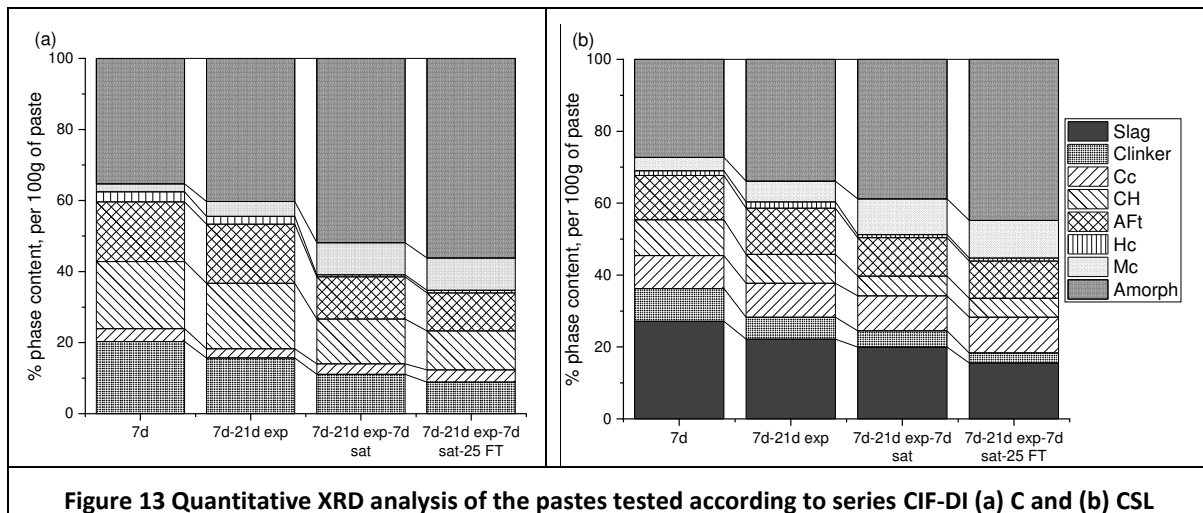
Figure 13 Quantitative XRD analysis of the pastes tested according to series CIF-DI (a) C and (b) CSL

Unlike series CIF, significant proportion of all phase assemblages were still present after 25 FT cycles and at comparable levels. This implies stability of phase assemblages at any stage depended largely on the microstructure presented. Moreover, carbonation appears to expose the inherent susceptibility of the limestone ternary cements (i.e. CSL) to decalcification.

3.2.3 Microstructure of cement pastes subjected to FT without carbonation nor leaching: series CIF-L

Phase assemblages

Series CIF and CIF-DI showed both cements to be susceptible to carbonation during equilibration, and decalcification upon capillary suction in deionized water. These phenomena altered the microstructures present at the start of the FT cycles. These changes were sufficiently significant so as to obscure assessment of the true performance of the cements against FT, although to a lesser extent compared to series CIF. Consequently, series CIF-L sought to evaluate the microstructure of the cements subjected to FT without carbonation nor leaching. Samples were cured as in series CIF-DI but capillary suction and FT exposure was performed in a saturated lime solution. The focus here is on the microstructures following the initial capillary suction and freeze-thaw in saturated lime solution.

From the DTG plots in Figure 14, the C-S-H and ettringite signals increased marginally after the 7d capillary suction and then after the 25 FT cycles irrespective of cement type. This is consistent with the observations in series CIF and CIF-DI. Unlike the other series however, the portlandite contents were stable in mix C but there was marginal consumption of portlandite as well as calcite noticed in CSL.
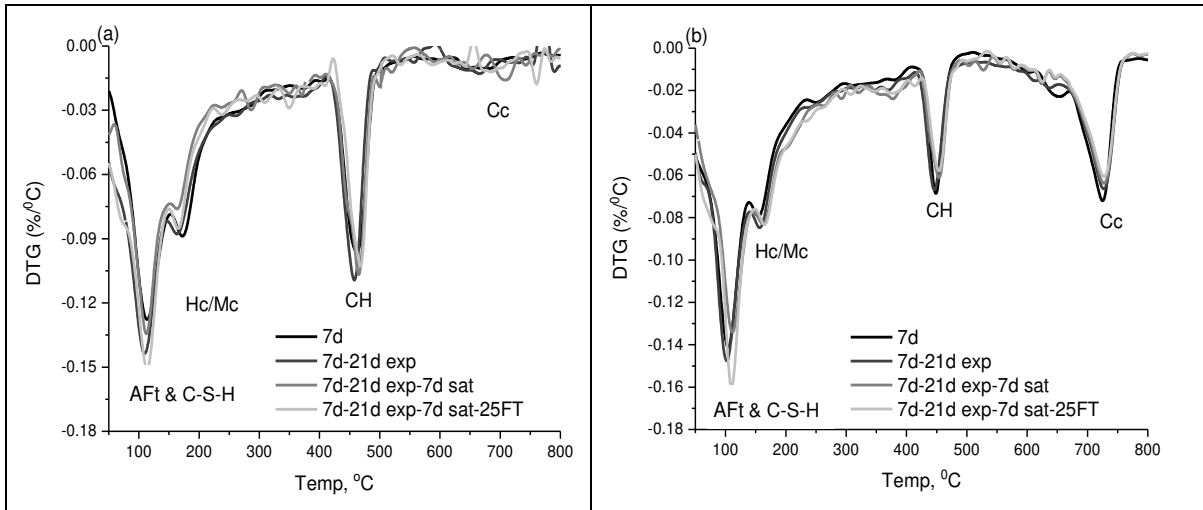
Figure 14 DTG plots of the series CIF-L samples (a) mix C, (b) mix CSL

387

The XRD plots in Figure 15 and QXRD in Figure 16 confirm ettringite stability after capillary
suction and exposure to the FT cycles. Similar to series CIF and CIF-DI, the QXRD results in
Figure 16 show increased XRD amorphous content, prominently after the 25th FT cycle.
Consequently, the increased signal at ~110°C (Figure 16) seems to be associated with
formation of additional C-S-H. Despite the prevalence of monocarboaluminates over hemi, the
Hc/Mc transformation was moderate compared to series CIF and CIF-DI where carbonation
and or leaching preceded the FT cycles. The Hc/Mc transition is consistent with the trends in
calcite consumption observed by TGA and XRD i.e. Figure 14 to 16.
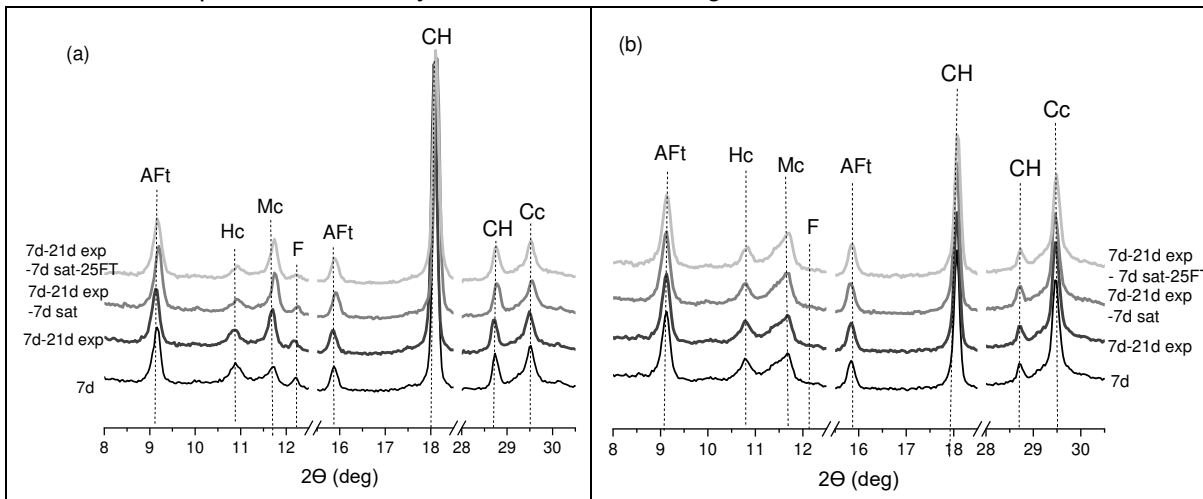
Figure 15 XRD plots of the series CIF-L samples (a) mix C, (b) mix CSL

396

Figure 16 (a and b) further indicates the progress of hydration during the initial capillary
suction, continuing through the FT cycles. Differences in the residual clinker contents in both
cements at the key stages were comparable among all three series.

400
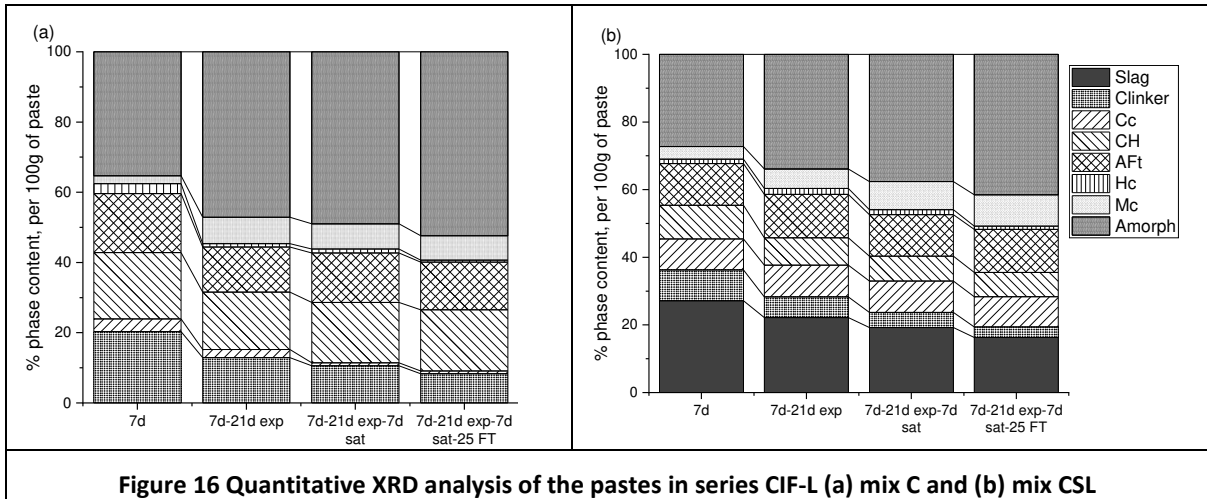
Figure 16 Quantitative XRD analysis of the pastes in series CIF-L (a) mix C and (b) mix CSL

401

Pore structure

402

403 Figure 17 (a and b) shows distribution of the accessible pores in mixes C and CSL at the key
404 stages of the FT test for series CIF-L (i.e. without exposing the cements to atmospheric CO_2
405 nor leachable test solution).

406 Compared to the pore distribution after 7-days, porosity reductions were noticed after 28-days
407 curing, caused by the additional hydrates. Herein, the extent of micro-capillary pore refinement
408 was greater than that induced by carbonation, as observed in series CIF. Capillary suction in
409 the lime solution reduced total porosity further but the affected pore ranges differed with the
410 cement type. The micro-capillary pores became dominant in mix C despite densification of
411 meso-pores. Conversely, gel and micro-capillary pores were refined in CSL with slight
412 increase in the threshold pore size due to dominance of meso-capillary pores.

413 Exposure to the FT cycles did not alter the pore distributions nor the total porosity significantly
414 in the ternary blend. However, there were slight modifications in the neat OPC mix. These
415 were in contrast with the post FT observations in the CIF series for the CSL samples, where
416 there was a significant increase in porosity. Notwithstanding the pore structural fluctuations
417 due to equilibration and saturation, the total porosity after 25 FT cycles were comparable for
418 each mix, with higher total porosity in the neat cement paste. These results reveal that
419 carbonation during the equilibration is antecedent to the heterogeneous pore structure.
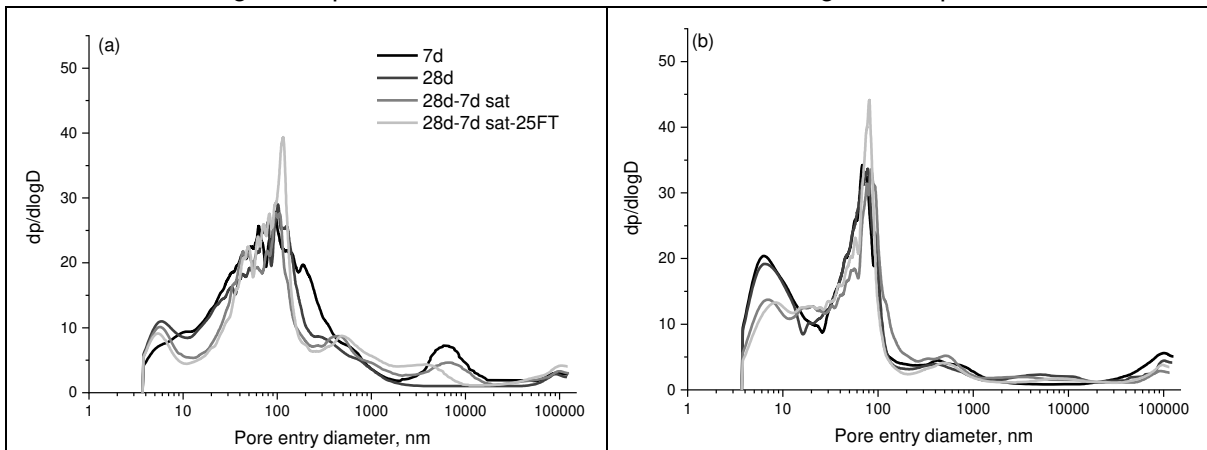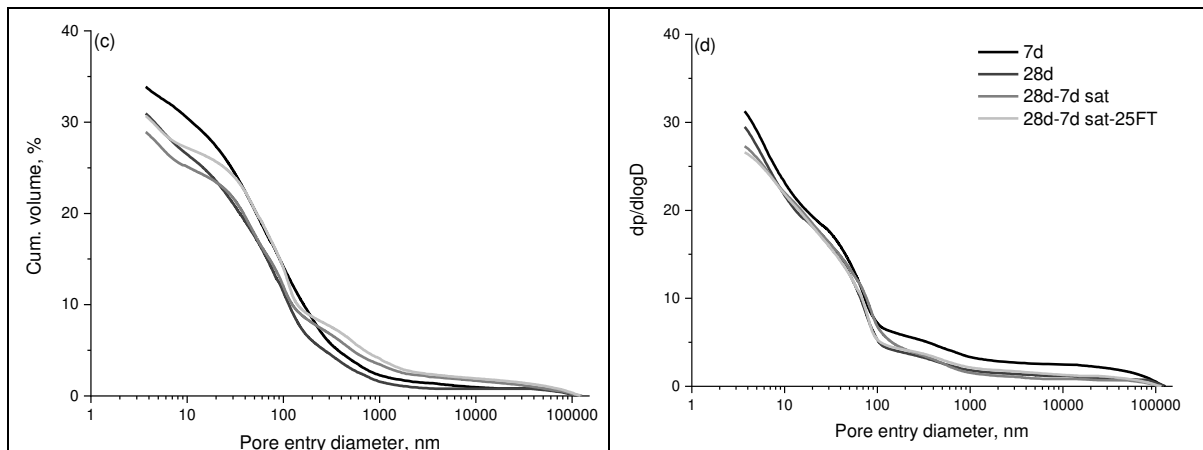
Figure 17 MIP measurement of cement paste samples tested according to series CIF-L

Note: (a) Pore distribution of Mix C, (b) pore distribution of mix CSL, (c) cumulative intruded volume in mix C and (d) cumulative intruded volume in mix CSL

420

3.3. Discussion

At the investigated 0.5w/c ratio, surface scaling and internal damage were greater in the composite cement concretes, including the limestone ternary cement mixes (Figure 5 and Figure 6). Characterization of the cement paste samples revealed marked differences in phase assemblages and pore structures when the samples partially carbonated during equilibration than those that didn't. The limestone ternary cement samples were more sensitive in this regard. Therefore, understanding the factors driving these changes offers new insight into the mechanism controlling their performance in the freeze-thaw test. The discussion that follows analyses these factors and evaluates the underlying mechanisms through which they potentially influenced freeze-thaw resistance and hence a hypothesis to explain susceptibility of the composite cements to this form of damage is proposed and validated on lab-scale concretes.

Hydration and microstructure development during equilibration

The microstructures, i.e. the degree of hydration, phase assemblages and porosity, at the start of FT cycles depended on the cement type, but the influence of the equilibrating environment was considerable. After 7d moist curing and start of equilibration, the degree of hydration of clinker in the CEM I and ternary cement is calculated to be 80 ±2%. Meanwhile, the degree of hydration of slag was approximately 35 ±5%, with limited consumption of limestone, as noticed in Figure 8 and 10. This means that overall degree of hydration in the ternary cement was ~55% compared to ~80% in the neat Portland cement, as shown in Figure 18, revealing an underdeveloped microstructure at the start of equilibration. This is not surprising and the controlling mechanisms are well understood [44, 55, 56]. However, the hydration degree and the pore structures at the beginning of exposure have significant implications on phase assemblage alterations arising from the equilibration.

Figure 18 shows the relationship between degree of hydration as determined from QXRD, bound water contents and total porosity. The figure shows continuing hydration during equilibration. There were good correlations amongst the samples that did not carbonate where porosity reduced and bound water increased with increasing hydration degree. For the partially

449 carbonated samples however, the bound water contents were lower in both cements than the
450 pre-equilibration levels. This mainly arose from drying and mild changes in the C-S-H, CH,
451 and AFt contents (see Figure 8 to 10). Meanwhile, porosity decreased in mix C due to the
452 combined effect of carbonation and hydration, while the total porosity increased in CSL. The
453 increased porosity and reducing bound water content may seem inconsistent with the progress
454 of hydration. Evaluation of the calcium hydroxide and carbonate contents before and after
455 equilibration however show greater degree of carbonation of calcium bearing hydrates i.e. C-
456 S-H and ettringite besides portlandite in mix CSL compared to C. These have larger molar
457 volumes than calcite and hence explain the increased porosity.

458 The question then arises as to how hydration progressed at 65% RH, contrary to the widely
459 held belief that hydration ceases below 80% RH [21, 57]. Hydration of clinker and slag at later
460 ages depend on pore solution chemistry, available space for hydrate growth, and internal
461 humidity [28, 29, 54, 58]. At the onset of equilibration, the microstructure is partially saturated,
462 allowing diffusion controlled hydration [59]. While most alite will have reacted by 7d [44], belite
463 and C_4AF, the dominant residual clinker minerals could still hydrate at 65% RH [60]. Moreover,
464 a moisture gradient between the outer surface and the core of the 1-2 mm crushed paste
465 samples, will allow self-desiccation and so further hydration. Furthermore, water is released
466 upon carbonation of portlandite and the C-S-H, and these may sustain hydration despite the
467 reduced relative humidity. Having said that, the water released upon carbonation may
468 eventually equilibrate with the ambient RH, and coarsening of the pore structure upon
469 carbonation, as shown in Figure 11 could facilitate evaporation, reducing the extent of
470 hydration and hence the bound water compared to those from series CIF-L, Figure 18.
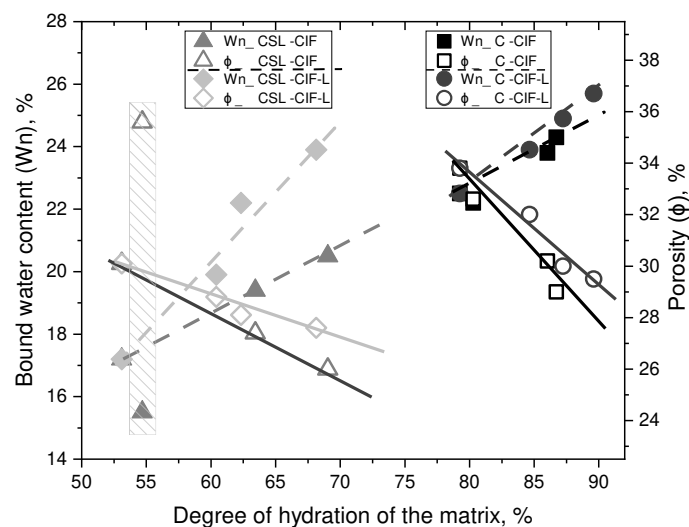
471

472 **Figure 18 Evolution of the degree of hydration, bound water and total porosity as a function of sample**
473 **equilibration and FT**

474 ### Renewed hydration and microstructure during capillary suction and FT

475 Saturating the cements in deionized water modified the microstructures, especially in the
476 partially carbonated limestone ternary cement sample (series CIF). Additional C-S-H,
477 ettringite, carboaluminates and calcite were confirmed in Figure 8 - 10, concurrent with the
478 loss/consumption of portlandite. These are consistent with the corresponding refinement of
479 gel-pores while meso and micro-capillary pores rather increased (see Figure 11). Important
480 questions therefore arise concerning these microstructural changes, e.g. was portlandite
481 consumed into other hydrates or leached into the test solution? If leaching occurred, then what

482 is the source of the additional ions that formed more hydrates, and what implications have
483 these alterations on the subsequent freeze-thaw resistance?

484 Increasing calcite contents after the initial 7-day capillary suction (Figure 8-10) suggest
485 crystallization of poorly crystalline calcium carbonate phases upon saturation, evident as a
486 shift towards higher temperature decomposition [61, 62]. Meanwhile, a high concentration of
487 calcium was noticed in the leachate (Figure 19). This implies portlandite was not only
488 consumed into additional hydrates but its solubility in the test environment [26, 63] caused
489 leaching. Leaching of calcium ions has also been reported in concrete dams experiencing
490 freeze-thaw damage [11]. Despite portlandite depletion in CSL, additional calcium was
491 detected in the test solution over the course of freeze-thaw cycles. The C-S-H Ca/Si
492 decreased accordingly in the ternary blended cement while that in the neat cement mix was
493 stable (Figure 21). This implies portlandite buffered decalcification of the C-S-H in the neat
494 cement during freeze-thaw as has been noted elsewhere upon carbonation [52, 64].

495 Calcium uptake into hydrates during capillary suction cannot be discounted. Hydration of
496 clinker (mainly C_2S) and slag during capillary suction were evident from Figure 10 and Figure
497 18 with increases in bound water contents plus pore refinement. Within the accuracy of the
498 QXRD/PONKCS technique [44], the unreacted clinker and slag contents were comparable
499 irrespective of the equilibration environment. This implies a more spontaneous rate of
500 hydration amongst the partially carbonated samples, particularly in the ternary cement and
501 thus explains the additionally formed hydrates.

502 Concerning ettringite, crystallinity is sensitive to relative humidity [22, 24] and its stability has
503 implication on the pore structure due to its large molar volume. Sulfates were detected in the
504 leachates only after the capillary suction as shown in Figure 19. Partial decomposition of
505 ettringite and the C-S-H signatures were noted after equilibration in atmospheric CO_2 (Figure
506 8) due to simultaneous carbonation and drying. It is thus reasonable to associate the additional
507 ettringite with sulfates evolved from carbonation of ettringite and potentially desorption from
508 the C-S-H. Modification of these during equilibration has been discussed in the preceding
509 section. It must be emphasised that the XRD data did not identify gypsum nor other crystalline
510 sulfate-bearing phases were detected after equilibration. Sulfate detection only after the initial
511 capillary suction, concomitant with the increasing ettringite content suggests these emerged
512 from amorphous water-soluble sulfate-bearing products, plausibly formed at the equilibration
513 stage. Meanwhile, secondary ettringite and AFm phases arising from portlandite dissolution
514 to maintain pore solution charge-balance has been suggested elsewhere [65].
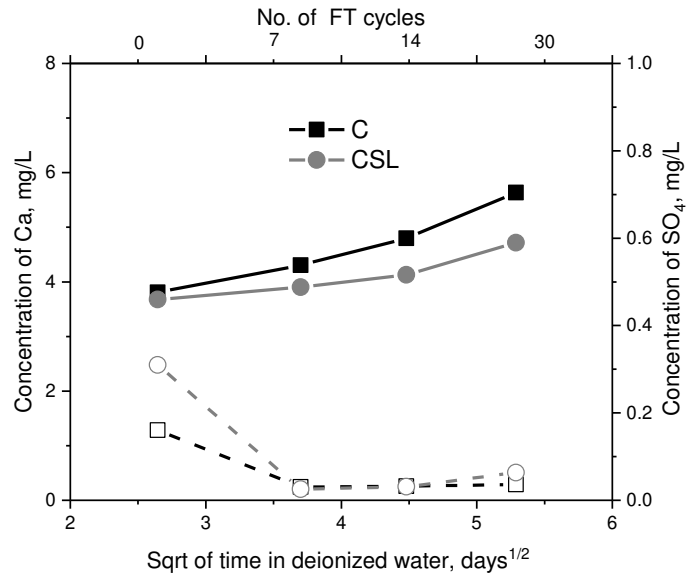
Figure 19 Concentration of calcium ions (solid lines) and sulfate ions (dashed lines) in the test solutions at various stages of the FT test as determined by Ion Chromatography.

Backscattered SEM images showing morphological changes in the C-S-H on the freezing fronts (corresponding to series CIF) compared to the core of the cements (series CIF-L) are shown in Figure 20. Unlike the neat cement, the partially carbonated and leached regions in the ternary cement was characterised by increased capillary porosity, consistent with the MIP results.
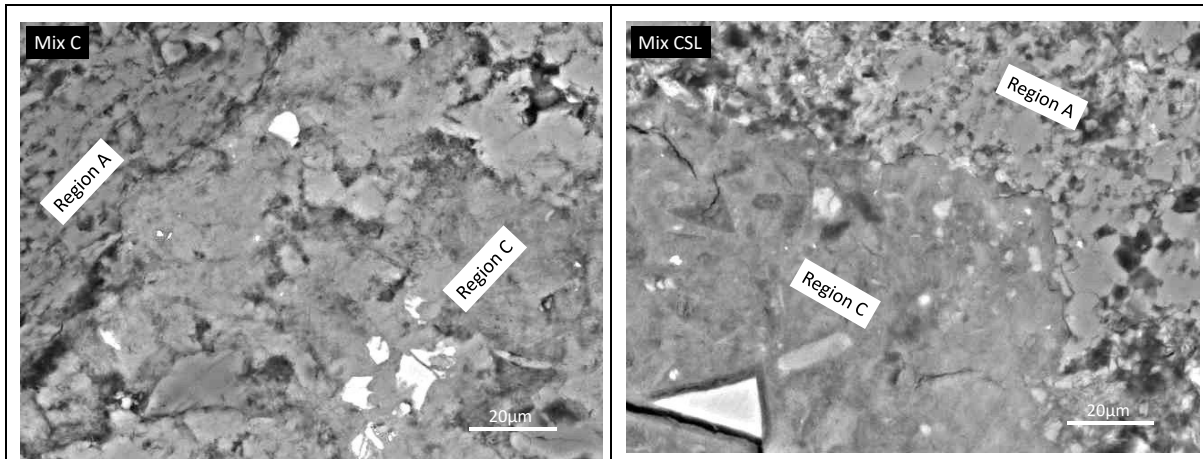
Figure 20 Backscattered SEM images showing the freezing front and the core of the cement samples for mixes C (left) and CSL (right)

Meanwhile, the C-S-H Ca/Si ratios were lower in the freezing front, confirming decalcification in both cements. The ternary cement inherently contained higher C-S-H S/Ca ratios, typical at 3 – 4% sulphate in the cement [66]. The S/Ca ratio did not change significantly after freeze-thaw. However, strong intermixing between the C-S-H and ettringite dominated the decalcified region in the ternary cement, Figure 21. The C-S-H/ettringite intermix, noticed only in the carbonated and leached ternary cement regions indicates possible late ettringite precipitation,

20

533 likely occurring in confined spaces within the C-S-H [67] which could also accelerate freeze-
534 thaw damage.
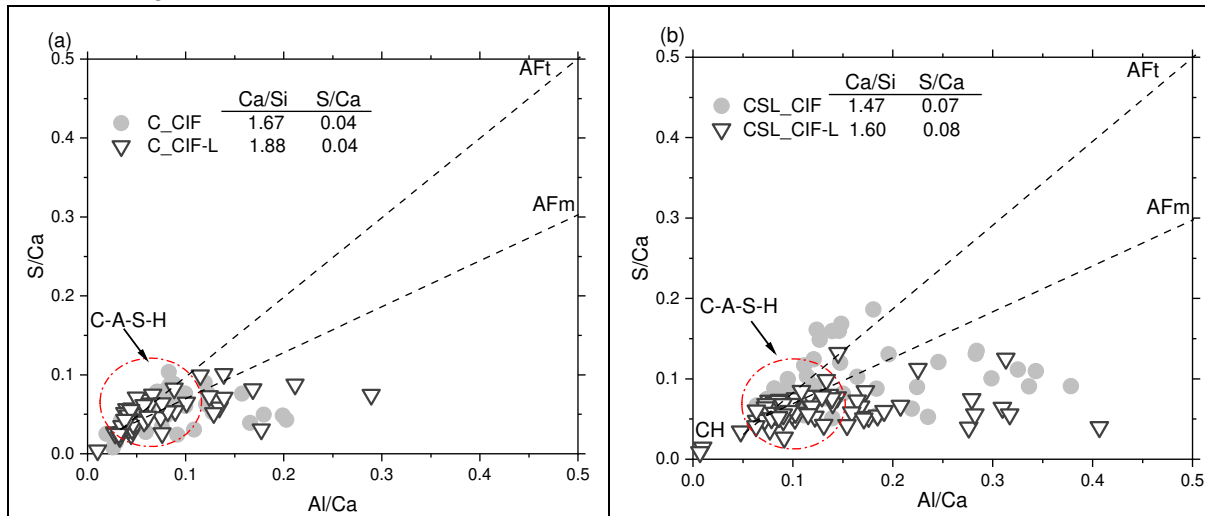
Figure 21 Composition of the C-S-H after 25FT cycles, tests conducted according to Series CIF and CIF-DI for (a) neat cement mix, C and (b) limestone ternary cement mix, CSL

Implication of the microstructural changes on freeze-thaw resistance and comparison with other postulated freeze-thaw damage mechanisms

539 Heterogeneous microstructures caused by the combination of carbonation, hydration, and
540 leaching, characterised the cements at the start of the FT cycles. These influenced the
541 subsequent freeze-thaw performance in two ways:

1. Increased permeability in the composite cement hydrated matrix and
2. Late precipitation of large-volume phase assemblages

544 Partial carbonation during equilibration reduced total porosity in the neat cement but that of
545 the limestone ternary cement increased. This agrees with observations in high SCM composite
546 cements reported elsewhere [30-32, 52, 64]. Leaching, during saturation of the samples
547 meanwhile increased capillary porosity despite refinement of gel pores and overall reduction
548 in total porosity (Figure 11). These changes reflected in a greater uptake of the test solution,
549 Figure 7, indicative of increased permeability in the composite cements including the limestone
550 ternary blends. Additionally, the MIP data show increased threshold pore diameters after
551 carbonation in both cements, Figure 22. It must be noted that composite cements are
552 inherently associated with lower threshold pore diameters [30, 31, 50]. Coarsening of the
553 pores during carbonation and leaching leads to more interconnecting pores than the neat
554 Portland cement. But, the proportion of gel and capillary pores, and their modification exert
555 even more significant influence on saturation, ice nucleation and growth. The CIF conditioning
556 regime altered the pores in this range significantly in the limestone ternary cement samples at
557 the start of the freeze-thaw cycles. Depending on the water to pore wall adhesion and pore
558 solution composition [6, 7], the test solution (deionized water in this case) infiltrating the gel
559 and meso-pores (<30nm) may also present a decreased freezing point or remain unfreezable
560 at low temperatures [68], increasing the ice-induced pressure at the freezing centres. These
561 changes are preceded by a more percolating matrix, accelerating the time to critical saturation
562 whilst coarsened capillary pores also increase the volume of freezing centres. Indeed, the FT
563 cycles induced additional meso/micro-capillary pores in all cements Figures 11 and 17. Such
564 pores saturate readily and serve as freezing centres [35, 68]. Therefore, the profound internal
565 damage and scaling in these (Figure 6) can be explained partly by the pore structural changes

21

566 occurring before and during the freeze-thaw cycles. That is, a more permeable microstructure
567 caused by carbonation and leaching is percolated during capillary suction with the dominant
568 meso-capillary pores becoming critically saturated and providing heterogeneous freezing
569 sites. Prevalence of saturated gel pores sustain the damage as the fluid migrates to the ice
570 nucleus in the larger pores [37]. This aligns with the hydraulic pressure theory [6, 36, 69],
571 which attributes freeze-thaw damage to saturated confined pores and their characteristics at
572 freezing temperatures. Specifically, the role of carbonation and leaching in modifying the pore
573 distribution and composition of the pore fluid (equilibrated with the phase assemblages) before
574 and during freeze-thaw cycles play an important role in freeze-thaw resistance.

575
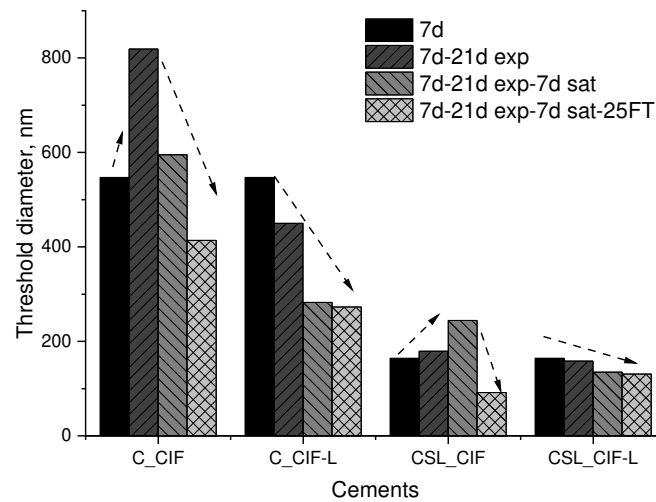
576 **Figure 22 Effect of cement type on the threshold pore diameter at the different stages of the test**

577

578 Crystallization pressure due to ice growth in confined pores is a recognized freeze-thaw
579 damage mechanism [7, 69]; the magnitude of which is a function of temperature, ice crystal
580 shape, and supersaturation [70]. The microanalysis data presented above revealed
581 precipitation of additional phase assemblages alongside ice crystals over the course of freeze-
582 thaw cycles. The additional hydration products were more pronounced in the partially
583 carbonated limestone ternary cement (see Figure 10 and 21). The origin of these additional
584 hydrates have been discussed above. Specifically, ettringite, carboaluminates, XRD
585 amorphous phases increased in addition to crystallisation of calcium carbonate. The
586 increasing volume fractions would also increase the crystallization pressure proportionate to
587 the molar volume of the crystals [67]. To precipitate ettringite and carboaluminates, the pore
588 solution must be saturated with respect to the contributing species (i.e. calcium, aluminium,
589 carbonates and sulfates). Not only do external sources of ions (e.g. chlorides) exert
590 crystallization pressure [70] but so do late dissolution and precipitation of hydrates [67]. This
591 implies that the later formed hydrates to an extent influenced the freeze-thaw resistance.
592 However, since neither crystalline gypsum nor monosulfoaluminate were noticed by XRD, it is
593 difficult to formulate the exact solubility product equations to estimate the magnitude of
594 crystallization pressures and hence this effect was not explored further. Notwithstanding, the
595 freeze-thaw cycles and hence ice growth already provides flaws in the matrix to allow the
596 generated pressure to propagate, contributing to damage of the concrete. This is consistent
597 with accelerated surface scaling due to freeze-thaw induced micro-cracks and its coupling with
598 external loads [38, 71].

599 The increasing capillary porosity and decalcification reflected on the micro-mechanical
600 properties of the pastes, as shown in Figure 23 for the partially carbonated cements before
601 and after the FT cycles. The modulus distribution is typical of cement hydrates [56, 57]. The
602 mean stiffness at the end of the equilibration was higher in the neat Portland cement (32
603 ±4GPa) compared to the ternary blend (~ 22 ±3GPa), explained in part by the inherently low
604 C-[A]-S-H Ca/Si in composite cements [58] and, by extension, carbonation. There was
605 evidence of portlandite after equilibration in both cements, but not in the ternary cement mix
606 after 25 FT cycles, consistent with the XRD and TGA data. Whereas stiffness of the low density
607 C-[A]-S-H in the ternary mix did not change significantly after freeze-thaw, that in the neat
608 cement shifted towards the low-density range. Decreasing micro-mechanical properties of
609 cement matrix upon freeze-thaw has been reported elsewhere [12, 13]. The observations here
610 indicate the significance of portlandite, plausibly restraining the C-S-H gel under stress
611 conditions. Since portlandite is stiffer than C-S-H, its depletion reduces the bulk modulus,
612 weakening the matrix and resistance to the pressure associated with ice growth.
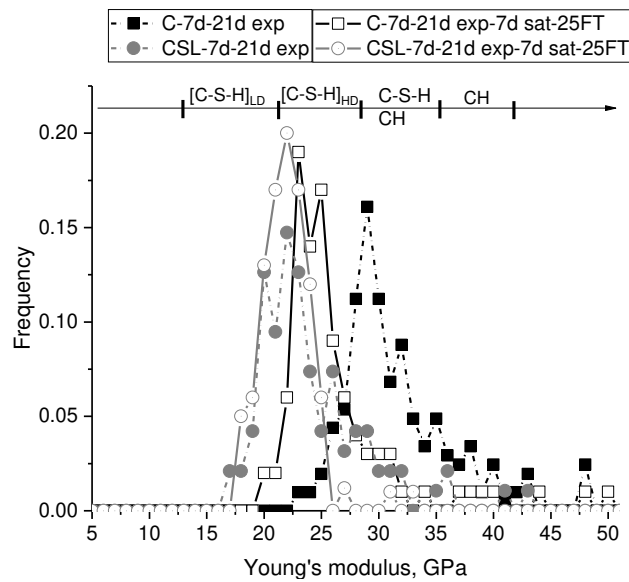
613

614 **Figure 23 Frequency density plot of the Young's modulus of carbonated and freeze-thawed pastes from**
615 **micro-indentation**

616 Note: Ranges corresponding to the different hydrates were taken from [46, 72].

Hypothesis for freeze-thaw damage in composite cements and validation in concrete

618 Based on the above discussion, it is hypothesized that the combined influence of carbonation
619 and leaching exacerbated freeze-thaw damage in the investigated composite cement
620 concrete. The C-S-H, ettringite and portlandite carbonated to a greater extent in the ternary
621 cement compared to the neat cement, resulting in a coarsening of the pore structures. Calcium
622 and sulphates leached into the test solution during capillary suction and freeze-thaw cycles
623 but at the same time additional phase assemblages formed. These changes, absent in the
624 samples that did not carbonate and leached, refined the nano-pores whilst the micro-pore
625 volume increased, consequently increasing suction capacity of the samples. Additionally,
626 portlandite depletion reduced matrix stiffness increasing susceptibility to freeze-thaw damage.

627 To evaluate the above hypothesis, concrete, made with the neat cement and the 10%
628 limestone ternary cement (i.e. C and CSL respectively), conditioned and tested without
629 carbonation during equilibration nor leaching during capillary suction and freeze-thaw (i.e.

corresponding to series CIF-L) were investigated. Figure 24 (a and b) shows representative photographs of the specimens after 56 FT cycles. Marked improvement in the scaling resistance is evident. Meanwhile, Figure 22 (c) indicates that internal damage still occurred but to a much lesser extent than in those reported in Figure 6, where the samples partially carbonated before saturation and freeze-thaw (i.e. the CIF regime).
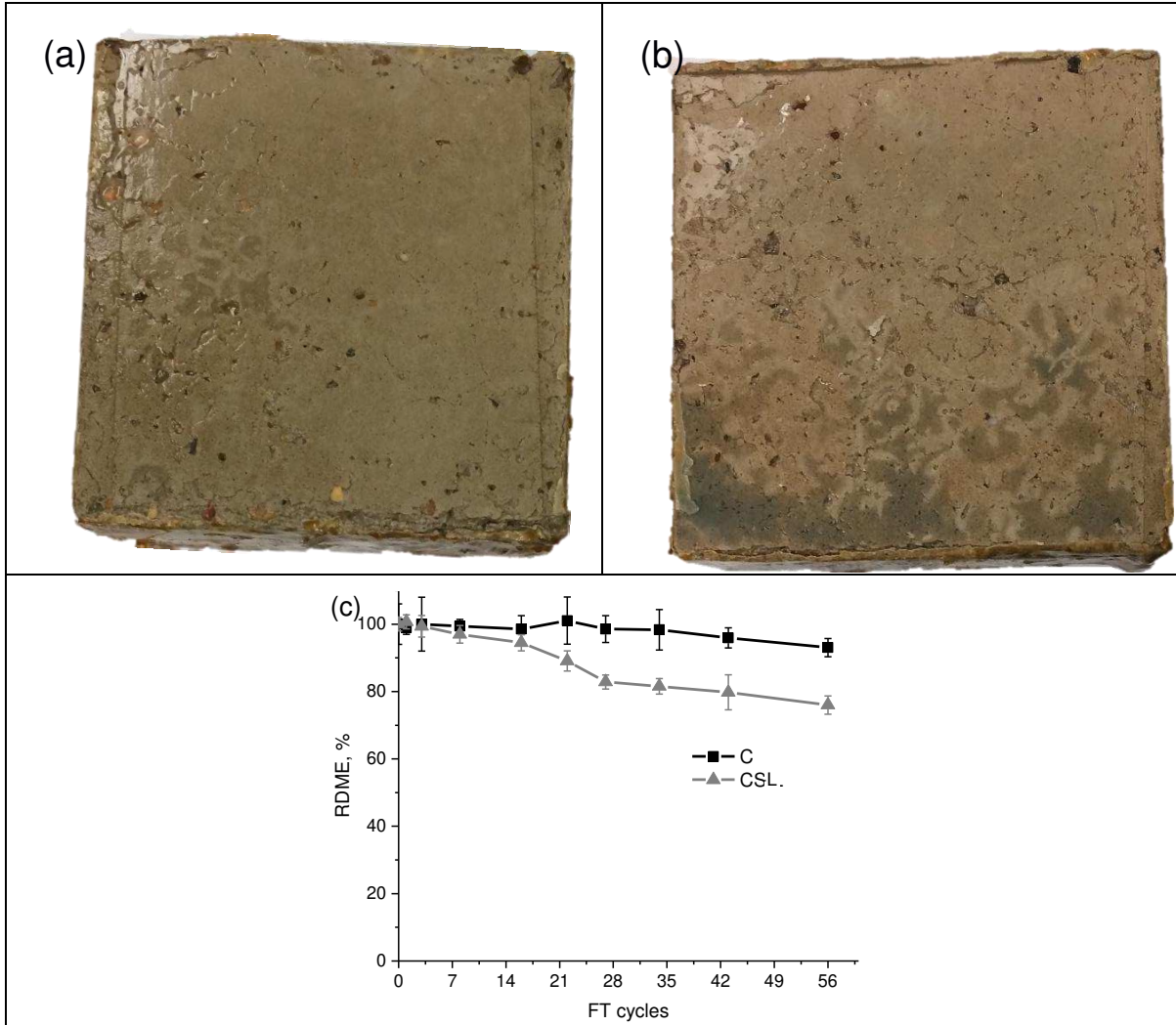
Figure 24 Effect of curtailed carbonation and leaching on freeze-thaw resistance of non-carbonated concrete (a) mix C after 56 FT cycles, (b) mix CSL after 56

4 Conclusions

We investigated internal damage and surface scaling of OPC and composite cement concretes and their complementary cement pastes subjected to freeze-thaw tests. The testing regime comprised exposure to natural CO_2 and saturating the samples in de-ionized water before exposure to the freeze-thaw cycles. The composite cement concretes (prepared at 50% replacement of OPC, 0.5 w/c ratio and without air entrainment) were more susceptible to deterioration. Comprehensive characterisation of the microstructures, including phase assemblages, pore structures and micro-mechanical property measurements, revealed defects caused by carbonation and leaching. The main conclusions are:

1. Combined carbonation and leaching led to pore structure changes, formation of new carbonation and hydration products, and loss through leaching of some phases. These

646 changes combined to render the concretes more susceptible to damage upon freeze-
647 thaw.
648 2. The inherently low portlandite contents in the composite cements with 50% clinker
649 substitution increased the carbonation risk of all calcium bearing hydrates. We
650 observed concurrent carbonation of ettringite and the C-S-H while some portlandite
651 was still present. Carbonation was more pronounced in the limestone ternary cement
652 and the porosity increased accordingly.
653 3. Capillary suction before and during the freeze-thaw cycles led to both continued
654 hydration and leaching of calcium, alkalis and sulfate ions. Loss of portlandite due to
655 leaching increased micro-capillary pore volume whilst simultaneous hydration further
656 refined the gel and meso-pores. The total porosity and threshold pore sizes decreased
657 accordingly in the neat cement paste. However, the partially carbonated limestone
658 ternary cement showed increasing percolation threshold diameter.
659 4. The poorly crystalline calcium carbonate formed during equilibration in an ambient CO_2
660 environment converted to calcite during freeze-thaw cycling, whilst more ettringite,
661 AFm and X-ray amorphous phases also formed per unit paste. These refined the pores
662 but their formation might also have contributed to the crystallization pressure in the
663 matrix.

664 The above findings demonstrate changes in the phase assemblages and pore structures due
665 to the test-conditioning regime of carbonation, leaching and hydration, which reduce
666 performance. Carbonation modified the phase assemblages and adversely increased porosity
667 in the ternary blended cement. Resumed hydration occurring simultaneously with leaching
668 during capillary suction altered the pore structure, becoming more heterogeneous in the
669 blended cement and accelerating damage, as demonstrated by improved performance when
670 samples were conditioned in limewater rather than deionised water. Therefore, freeze-thaw
671 deterioration should be considered as more than purely a physical phenomenon, being
672 affected by phase changes also.

References

674 [1] J. Marchand, M. Pigeon, D. Bager, C. Talbot, Influence of Chloride Solution
675 Concentration on Deicer Salt Scaling Deterioration of Concrete, Materials Journal,
676 96 (1999) 429-435.

677 [2] J.J. Valenza, G.W. Scherer, A review of salt scaling: I. Phenomenology, Cement
678 and Concrete Research, 37 (2007) 1007-1021.

679 [3] J. Stark, H.M. Ludwig, Freeze-Thaw and Freeze-Deicing Salt Resistance of
680 Concretes Containing Cement Rich in Granulated Blast Furnace Slag, Materials
681 Journal, 94 (2002) 47-55.

682 [4] J. Marchand, Y. Maltais, Y. Machabee, C. TAlbot, M. Pigeon, Effects of Fly ash
683 on microstructure and deicer salt scaling resistance of concrete, in: M.J. Setzer, R.
684 Auberg (Eds.) Frost Resistance of Concrete: Proceedings of the International
685 RILEM Workshop, E & FN SPN1997, pp. 21-30.

686 [5] P. Michel Pigeon. Jacaues, S. Jean-Marc, Freeze-Thaw Durablity Versus
687 Freezing Rates, Journal Proceedings, 82 (1985) 684-692.

688 [6] T.C. Powers, R.A. Helmuth, Theory of volume changes in hardened Portland
689 cement paste during freezing, Highway Research Board, 32 (1953).

690 [7] J.J. Valenza, G.W. Scherer, Mechanism for Salt Scaling, Journal of the American
691 Ceramic Society, 89 (2006) 1161-1179.

692 [8] J. Marchand, Y. Maltais, Y. Machabee, C. TAlbot, M. Pigeon, Effects of fly ash on
693 microstructure and deicer salt scaling resistance of concrete, in: M.J. Setzer, R.
694 Auberg (Eds.) Frost Resistance of Concrete. Proceedings of the International
695 RILEM WorkshopUniversity of Essen, 1997, pp. 11 - 20.

696 [9] J. Deja, Freezing and de-icing salt resistance of blast furnace slag concretes,
697 Cement and Concrete Composites, 25 (2003) 357-361.

698 [10] X. Shi, L. Fay, M.M. Peterson, Z. Yang, Freeze–thaw damage and chemical
699 change of a portland cement concrete in the presence of diluted deicers, Materials
700 and Structures 43 (2010) 933-946

701 [11] M. Rosenqvist, L.W. Pham, A. Terzic, K. Fridh, M. Hassanzadeh, Effects of
702 interactions between leaching, frost action and abrasion on the surface deterioration
703 of concrete, Construction and Building Materials, 149 (2017) 849-860.

704 [12] P. Zhang, F.H. Wittmann, M. Vogel, H.S. Müller, T. Zhao, Influence of freeze-
705 thaw cycles on capillary absorption and chloride penetration into concrete, Cement
706 and Concrete Research, 100 (2017) 60-67.

707 [13] L. Liu, X. Wang, J. Zhou, H. Chu, D. Shen, H. Chen, S. Qin, Investigation of
708 pore structure and mechanical property of cement paste subjected to the coupled
709 action of freezing/thawing and calcium leaching, Cement and Concrete Research,
710 109 (2018) 133-146.

711 [14] R. Bleszynski, D. Hooton, M.D.A. Thomas, C.A. Rogers, Durability of Ternary
712 Blend Concrete with Silica Fume and Blast-Furnace Slag: Laboratory and Outdoor
713 Exposure Site Studies, Materials Journal, 99 (2002).

714 [15] G.J. Osborne, Durability of Portland blast-furnace slag cement concrete,
715 Cement and Concrete Composites, 21 (1999) 11-21.

716 [16] M.D.A. Thomas, A. Scott, T. Bremner, A. Bilodeau, D. Day, Performance of Slag
717 Concrete in Marine Environment, Materials Journal, 105 (2008) 628-634.

718 [17] S. Tsivilis, G. Batis, E. Chaniotakis, G. Grigoriadis, D. Theodossis, Properties
719 and behavior of limestone cement concrete and mortar, Cement and Concrete
720 Research, 30 (2000) 1679-1683.

721 [18] R.K. Dhir, M.C. Limbachiya, M.J. Macarthy, A. Chaipanich, Evaluation of
722 Portland limestone cements for use in concrete construction, Materials and
723 Structures, 40 (2007) 459 - 473.

724 [19] H. Kuosa, R.M. Ferreira, E. Holt, M. Leivo, E. Vesikari, Effect of coupled
725 deterioration by freeze–thaw, carbonation and chlorides on concrete service life,
726 Cement and Concrete Composites, 47 (2014) 32-40.

727 [20] O.M. Jensen, P.F. Hansen, E.E. Lachowski, F.P. Glasser, Clinker mineral
728 hydration at reduced relative humidities, Cement and Concrete Research, 29 (1999)
729 1505-1512.

730 [21] M. Wyrzykowski, P. Lura, Effect of relative humidity decrease due to self-
731 desiccation on the hydration kinetics of cement, Cement and Concrete Research, 85
732 (2016) 75-81.

733 [22] G. Renaudin, Y. Filinchuk, J. Neubauer, F. Goetz-Neunhoeffer, A comparative
734 structural study of wet and dried ettringite, Cement and Concrete Research, 40
735 (2010) 370-375.

736 [23] L.G. Baquerizo, T. Matschei, K.L. Scrivener, M. Saeidpour, L. Wadsö, Hydration
737 states of AFm cement phases, Cement and Concrete Research, 73 (2015) 143-157.

738 [24] L.G. Baquerizo, T. Matschei, K.L. Scrivener, Impact of water activity on the
739 stability of ettringite, Cement and Concrete Research, 79 (2016) 31-44.

740 [25] L. Zhang, F.P. Glasser, Critical examination of drying damage to cement pastes,
741 Advances in Cement Research, 12 (2000) 79-88.

742 [26] C. Carde, R. François, Effect of the leaching of calcium hydroxide from cement
743 paste on mechanical and physical properties, Cement and Concrete Research, 27
744 (1997) 539-550.

745 [27] K. Haga, S. Sutou, M. Hironaga, S. Tanaka, S. Nagasaki, Effects of porosity on
746 leaching of Ca from hardened ordinary Portland cement paste, Cement and
747 Concrete Research, 35 (2005) 1764-1775.

748 [28] K. Scrivener, B. Lothenbach, N. De Belie, E. Gruyaert, J. Skibsted, R. Snellings,
749 A. Vollpracht, TC 238-SCM: Hydration and microstructure of concrete with SCMs,
750 Materials and Structures, 48 (2015) 835-862.

751 [29] K.L. Scrivener, A. Nonat, Hydration of cementitious materials, present and
752 future, Cement and Concrete Research, 41 (2011) 651-665.

753 [30] B. Wu, G. Ye, Development of porosity of cement paste blended with
754 supplementary cementitious materials after carbonation, Construction and Building
755 Materials, 145 (2017) 52-61.

756 [31] A. Younsi, P. Turcry, A. Aït-Mokhtar, S. Staquet, Accelerated carbonation of
757 concrete with high content of mineral additions: Effect of interactions between
758 hydration and drying, Cement and Concrete Research, 43 (2013) 25-33.

759 [32] Z. Shi, B. Lothenbach, M.R. Geiker, J. Kaufmann, A. Leemann, S. Ferreiro, J.
760 Skibsted, Experimental studies and thermodynamic modeling of the carbonation of
761 Portland cement, metakaolin and limestone mortars, Cement and Concrete
762 Research, 88 (2016) 60-72.

763 [33] S. Steiner, B. Lothenbach, T. Proske, A. Borgschulte, F. Winnefeld, Effect of
764 relative humidity on the carbonation rate of portlandite, calcium silicate hydrates and
765 ettringite, Cement and Concrete Research, 135 (2020) 106116.

766 [34] X. Shi, L. Fay, M.M. Peterson, Z. Yang, Freeze–thaw damage and chemical
767 change of a portland cement concrete in the presence of diluted deicers, Materials
768 and Structures, 43 (2010) 933-946.

769 [35] G. Fagerlund, Internal frost attack - State of the art, in: M.J. Setzer, R. Auberg
770 (Eds.) Frost Resistance of Concrete. Proceedings of the International RILEM
771 WorkshopEssen, 1997, pp. 321 - 338.

772 [36] T.C. Powers, A Working Hypothesis for Further Studies of Frost Resistance of
773 Concrete, ACI Journal Proceedings, 41 (1945) 245-272.

774 [37] M.J. Setzer, Micro-Ice-Lens Formation in Porous Solid, Journal of Colloid and
775 Interface Science, 243 (2001) 193-201.

776 [38] O. Çopuroğlu, E. Schlangen, Modeling of frost salt scaling, Cement and
777 Concrete Research, 38 (2008) 27-39.

778 [39] R.J. Detwiler, B.J. Dalgleish, R.B. Williamson, Assessing the durability of
779 concrete in freezing and thawing, ACI Materials Journal, 86 (1989) 29-35.

780 [40] D.J. Corr, P.J.M. Monteiro, J. Bastacky, Microscopic Characterization of Ice
781 Morphology in Entrained Air Voids, ACI Materials Journal, 99 (2002) 190-195.

782 [41] A.I. Rashed, R.B. Williamson, Microstructure of entrained air voids in concrete,
783 Part I, Journal of Materials Research, 6 (2011) 2004-2012.

784 [42] PDCEN/TR15177, Testing the freeze-thaw resistance of concrete-Internal
785 structural damage, 2006.

786 [43] R. Auberg, M.J. Setzer, Influence of water uptake during freezing and thawing,
787 in: M.J.S. R. Auberg (Ed.) Frost Resistance of Concrete Proceedings of the
788 International RILEM Workshop, E&FN SPON, 1997, pp. 232-242.

789 [44] S. Adu-Amankwah, M. Zajac, C. Stabler, B. Lothenbach, L. Black, Influence of
790 limestone on the hydration of ternary slag cements, Cement and Concrete Research,
791 100 (2017) 96-109.

792 [45] J.Č. Borislav Zdravkov , Martin Šefara and Josef Janků, Pore classification in
793 the characterization of porous materials: A perspective, ntral European Journal of
794 Chemistry, 5 (2007) 385 - 395.

795 [46] J. Němeček, Creep effects in nanoindentation of hydrated phases of cement
796 pastes, Materials Characterization, 60 (2009) 1028-1034.

797 [47] W.C. Oliver, G.M. Pharr, An improved technique for determining hardness and
798 elastic modulus using load and displacement sensing indentation experiments, J
799 Mater Res, (1992) 1564-1583.

800 [48] M.J. Setzer, P. Heine, S. Kasparek, S. Palecki, R. Auberg, V. Feldrappe, E.
801 Siebel, Test methods for frost resistance of concrete: CIF Test: Capillary suction,
802 Internal damage and freeze thaw test - Referennce method and alternative methods
803 A and B, Materials and Structures, 37 (2004) 743 - 753.

804 [49] S. Adu-Amankwah, M. Zajac, J. Skocek, M.B. Haha, L. Black, Relationship
805 between cement composition and the freeze–thaw resistance of concretes,
806 Advances in Cement Research, 30 (2018) 387-397.

807 [50] M. Zajac, J. Skocek, S. Adu-Amankwah, L. Black, M. Ben Haha, Impact of
808 microstructure on the performance of composite cements: Why higher total porosity
809 can result in higher strength, Cement and Concrete Composites, 90 (2018) 178-192.

810 [51] A. Morandeau, M. Thiéry, P. Dangla, Investigation of the carbonation
811 mechanism of CH and C-S-H in terms of kinetics, microstructure changes and
812 moisture properties, Cement and Concrete Research, 56 (2014) 153-170.

813 [52] A. Morandeau, M. Thiéry, P. Dangla, Impact of accelerated carbonation on OPC
814 cement paste blended with fly ash, Cement and Concrete Research, 67 (2015) 226-
815 236.

816 [53] E. Dubina, J. Plank, L. Korat, J. Strupi-Suput, L. Black, Influence of Water
817 Vapour and Carbon Dioxide on Free Lime During Storage at 80oC, studied by
818 Raman spectroscopy, Spectrochimica Acta - Part A Molecular and Biomolecular
819 Spectroscopy, 111 (2013) 299-303.

820 [54] E. Berodier, K. Scrivener, Evolution of pore structure in blended systems,
821 Cement and Concrete Research, 73 (2015) 25-35.

822 [55] A. Arora, G. Sant, N. Neithalath, Ternary blends containing slag and
823 interground/blended limestone: Hydration, strength, and pore structure, Construction
824 and Building Materials, 102 (2016) 113-124.

825 [56] K. De Weerdt, M. Ben Haha, G. Le Saout, K.O. Kjellsen, H. Justnes, B.
826 Lothenbach, Hydration mechanisms of ternary Portland cements containing
827 limestone powder and fly ash, Cement and Concrete Research, 41 (2011) 279-291.

828 [57] R.G. Patel, D.C. Killoh, L.J. Parrott, W.A. Gutteridge, Influence of curing at
829 different relative humidities upon compound reactions and porosity in Portland
830 cement paste, Materials and Structures, 21 (1988) 192-197.

831 [58] K.A. Snyder, D.P. Bentz, Suspended hydration and loss of freezable water in
832 cement pastes exposed to 90% relative humidity, Cement and Concrete Research,
833 34 (2004) 2045-2056.

834 [59] M. Zajac, J. Skocek, B. Lothenbach, B.H. Mohsen, Late hydration kinetics:
835 Indications from thermodynamic analysis of pore solution data, Cement and
836 Concrete Research, 129 (2020) 105975.

837 [60] O.M. Jensen, Thermodynamic limitation of self-desiccation, Cement and
838 Concrete Research, 25 (1995) 157-164.

839 [61] T. Ogino, T. Suzuki, K. Sawada, The formation and transformation mechanism
840 of calcium carbonate in water, Geochimica et Cosmochimica Acta, 51 (1987) 2757-
841 2767.

842 [62] P. López-Arce, L.S. Gómez-Villalba, S. Martínez-Ramírez, M. Álvarez de
843 Buergo, R. Fort, Influence of relative humidity on the carbonation of calcium
844 hydroxide nanoparticles and the formation of calcium carbonate polymorphs, Powder
845 Technology, 205 (2011) 263-269.

846 [63] C. Carde, R. François, Modelling the loss of strength and porosity increase due
847 to the leaching of cement pastes, Cement and Concrete Composites, 21 (1999) 181-
848 188.

849 [64] V. Shah, K. Scrivener, B. Bhattacharjee, S. Bishnoi, Changes in microstructure
850 characteristics of cement paste on carbonation, Cement and Concrete Research,
851 109 (2018) 184-197.

852 [65] P. Faucon, F. Adenot, M. Jorda, R. Cabrillac, Behaviour of crystallised phases of
853 Portland cement upon water attack, Materials and Structures, 30 (1997) 480-485.

854 [66] C. Famy, A.R. Brough, H.F.W. Taylor, The C-S-H gel of Portland cement
855 mortars: Part I. The interpretation of energy-dispersive X-ray microanalyses from
856 scanning electron microscopy, with some observations on C-S-H, AFm and AFt
857 phase compositions, Cement and Concrete Research, 33 (2003) 1389-1398.

858 [67] R.J. Flatt, G.W. Scherer, Thermodynamics of crystallization stresses in DEF,
859 Cement and Concrete Research, 38 (2008) 325-336.

860 [68] M.J. Setzer, Basis of testing the freeze-thaw resistance: surface and internal
861 deterioration, in: M.J. Setzer, R. Auberg (Eds.) RILEM Proceedings Frost Resistance
862 of Concrete, E&FN Spon, 1997, pp. 157-173.

863   [69] O. Coussy, Poromechanics of freezing materials, Journal of the Mechanics and
864   Physics of Solids, 53 (2005) 1689-1718.

865   [70] G.W. Scherer, Crystallization in pores, Cement and Concrete Research, 29
866   (1999) 1347-1358.

867   [71] Y. Cheng, Y. Zhang, Y. Jiao, J. Yang, Quantitative analysis of concrete property
868   under effects of crack, freeze-thaw and carbonation, Construction and Building
869   Materials, 129 (2016) 106-115.

870   [72] L. Sorelli, G. Constantinides, F.-J. Ulm, F. Toutlemonde, The nano-mechanical
871   signature of Ultra High Performance Concrete by statistical nanoindentation
872   techniques, Cement and Concrete Research, 38 (2008) 1447-1456.

873